



Mineralization of organic matter in boreal lake sediments: Rates, pathways and nature of the fermenting substrates

François Clayer^{1,3}, Yves Gélinas^{2,3}, André Tessier¹, Charles Gobeil^{1,3}

¹INRS-ETE, Université du Québec, 490 rue de la Couronne, Québec (QC), Canada G1K 9A9

5 ²Concordia University, Department of Chemistry and Biochemistry, 7141 Sherbrooke Street West, Montreal (QC), Canada H4B 1R6

³Geotop, Interuniversity research and training centre in geosciences, 201 Président-Kennedy Ave., Montréal (QC), Canada H2X 3Y7

Correspondence to: François Clayer (francois.clayer@niva.no)

10 **Abstract.** The complexity of organic matter (OM) degradation mechanisms represents a significant challenge for developing biogeochemical models to quantify the role of aquatic sediments in the climate system. The common representation of OM by carbohydrates formulated as CH₂O in models comes with the assumption that its degradation by fermentation produces equimolar amounts of methane (CH₄) and dissolved inorganic carbon (DIC). To test the validity of this assumption, we modeled using reaction-transport equations vertical profiles of the concentration and isotopic composition ($\delta^{13}\text{C}$) of CH₄ and
15 DIC in the top 25 cm of the sediment column from two lake basins, one whose hypolimnion is perennially oxygenated and one with seasonal anoxia. Our results reveal that methanogenesis only occurs via hydrogenotrophy in both basins. Furthermore, we calculate, from CH₄ and DIC production rates associated with methanogenesis, that the fermenting OM has an average carbon oxidation state (COS) below -0.9 . Modeling solute porewater profiles reported in the literature for four other seasonally anoxic lake basins also yields negative COS values. Collectively, the mean (\pm SD) COS value of -1.4 ± 0.3 for all the seasonally
20 anoxic sites is much lower than the value of zero expected from carbohydrates fermentation. We conclude that carbohydrates do not adequately represent the fermenting OM and that the COS should be included in the formulation of OM fermentation in models applied to lake sediments. This study highlights the need to better characterize the labile OM undergoing mineralization to interpret present-day greenhouse gases cycling and predict its alteration under environmental changes.

1 Introduction

25 Significant proportions of atmospheric methane (CH₄) and carbon dioxide (CO₂), two powerful greenhouse gases, are thought to originate from freshwater lake sediments (Wuebbles and Hayhoe 2002; Bastviken et al., 2004; Turner et al., 2015), but large uncertainties remain concerning their contribution to the global CO₂ and CH₄ budgets (Saunio et al., 2016). The role of these waterbodies in the global carbon (C) budget has been acknowledged for more than a decade (Cole et al. 2007). Especially in the lake-rich boreal region, lakes are hotspots of CO₂ and CH₄ release (Hastie et al., 2018; Wallin et al., 2018) and intensive
30 sites of terrestrial C processing (Holgerson and Raymond, 2016; Staehr et al., 2012). Using high-resolution satellite imagery,



Verpoorter et al. (2014) estimated to about 27 million the number of lakes larger than 0.01 km² on Earth and reported that the highest lake concentration and surface area are found in boreal regions. Boreal lakes, which are typically small and shallow, are known to store large amounts of organic C, to warm up quickly, and to develop anoxic hypolimnia in the warm season (Schindler et al., 1996; Sabrekov et al., 2017). Owing to the great abundance of boreal lakes, their sensitivity to climate change and foreseen important role in the global C cycle, there is a need to further develop process-based models to better quantify C processing reactions in these lakes and their alteration under warming (Saunois et al., 2016).

In aquatic environments, CH₄ is mainly produced (methanogenesis) in the sediment along with CO₂ at depths where most electron acceptors (EAs) are depleted (Conrad, 1999; Corbett et al., 2013). During its upward migration to the atmosphere, CH₄ is partly aerobically or anaerobically oxidized to CO₂ (methanotrophy) in the upper strata of the sediments and in the water column (Bastviken et al., 2008; Raghoebarsing et al. 2006; Beal et al. 2009; Ettwig et al. 2010; Egger et al. 2015). The oxidation of organic matter (OM) by EAs such as O₂, NO₃⁻, Fe(III), Mn(IV), SO₄²⁻ and humic substances, as well as the partial fermentation of high molecular weight organic matter (HMW OM) into lower molecular weight organic matter (LMW OM) are also potential sources of CO₂ in the sedimentary environment (Corbett et al., 2015). Predicting fluxes of CH₄ and CO₂ from the aquatic sediments and water column to the atmosphere is challenging considering the various transport processes and chemical and microbially-mediated reactions implicated and the complexity of natural OM which serves as substrate (Natchimuthu et al., 2017).

Process-based geochemical models taking into account both the numerous biogeochemical reactions involving C and transport processes are powerful tools able to interpret present-day sediment, porewater and water-column profiles of C species and offer a great potential to forecast changes in cycling of this element under variable environmental scenarios (Wang and Van Cappellen 1996; Arndt et al., 2013; Paraska et al., 2014; Saunois et al., 2016). Nonetheless, the performance of these models depends on the correct formulation of the OM mineralization reactions, particularly in terms of the metabolizable organic compounds involved. Up to now, carbohydrates, represented as the simple chemical formula CH₂O (or C₆H₁₂O₆), whose average carbon oxidation state (COS) is zero, are commonly assumed to be representative of the bulk of metabolizable OM, including the substrates involved in fermentation reactions (e.g., Arndt et al., 2013; Paraska et al., 2014; Arning et al., 2016 and references therein). The capacity of CH₂O to represent adequately the ensemble of labile organic compounds is, nevertheless, becoming increasingly questioned in the literature given the variety and complexity of organic molecules present in the environment (Alperin et al., 1994; Berelson et al., 2005; Jørgensen and Parkes, 2010; Burdige and Komada, 2011; Clayer et al., 2016). Based on the observation that methanogenesis produced CH₄ three times faster than CO₂ in the sediments of a boreal, sporadically anoxic lake basin, Clayer et al. (2018) concluded that the fermenting OM had a markedly negative COS value of -1.9. This COS value corresponds more closely to a mixture of fatty acids and fatty alcohols than to carbohydrates (e.g., CH₂O), which would have yielded equivalent CH₄ and CO₂ production rates. The low COS value of metabolizable OM in the sediment layer where methanogenesis occurred in this lake has been attributed to the nearly complete consumption of the most labile organic components (e.g., carbohydrates, proteins) during its downward transport through the water column and the upper sediment layers, thus leaving only material of lower lability such as fatty acids and fatty alcohols available for



65 methanogenesis. Such interpretation, however, must be validated by investigating other lakes before revising the formulation of the fermenting OM used in diagenetic models in order to improve model predictions of C cycling, including greenhouse gases production and emission from these environments.

In this study, centimeter-scale vertical porewater profiles of the concentrations and of the stable carbon isotope ratios ($\delta^{13}\text{C}$) of CH_4 and dissolved inorganic carbon (DIC), as well as those of the concentrations of EAs were obtained in the hypolimnetic
70 sediments of two additional boreal lake basins showing contrasted O_2 dynamics: one whose hypolimnion remains perennially oxygenated and the other whose hypolimnion becomes anoxic for several months annually. Reaction-transport equations are used to quantify the rates of each OM mineralization pathway and estimate the COS of the substrates fermenting in the sediments. Additional insight into the COS of the fermenting OM in lakes is also provided by applying these equations to similar porewater solute concentration profiles gathered from the scientific literature or from our data repository.

75 2 Materials and Methods

2.1 Sites and sample collection

This study was carried out in two small, dimictic, oligotrophic and headwater lakes located within 50 km from Québec City, Eastern Canada and having fully forested and uninhabited watersheds (Fig. 1). Lake Tantaré ($47^{\circ}04'\text{N}$, $71^{\circ}32'\text{W}$) is part of the Tantaré Ecological Reserve and has four basins connected by shallow channels and a total surface area of 1.1 km^2 . Lake
80 Bédard ($47^{\circ}16'\text{N}$, $71^{\circ}07'\text{W}$), lying in the protected Montmorency Forest, comprises only one small (0.05 km^2) basin. The samples for this study were collected at the deepest sites of Lake Bédard (10 m) and of the westernmost basin of Lake Tantaré (15 m), thereafter referred to as Basin A of Lake Tantaré to remain consistent with our previous studies (e.g., Couture et al., 2008; Clayer et al., 2016). These two sampling sites were selected based on their contrasting O_2 regimes (Fig. 1): Lake Bédard develops an anoxic hypolimnion early in the summer (D'arcy, 1993), whereas the hypolimnion of Lake Tantaré Basin A is
85 perennially oxygenated (Couture et al., 2008). The O_2 diffusion depth in the sediments of Lake Tantaré Basin A, as measured with a microelectrode, does not exceed 4 mm (Couture et al., 2016).

Sediment porewater samples were acquired by *in situ* dialysis in October 2015 with peepers (Hesslein, 1976; Carignan et al., 1985) deployed by divers within a 25-m^2 area at the deepest site of each lake basin. Bottom water O_2 concentrations were ~ 2.5 and $< 0.1 \text{ mg L}^{-1}$ in Lake Tantaré Basin A and in Lake Bédard, respectively. The acrylic peepers comprised two columns of
90 4-mL cells, filled with ultrapure water, and covered by a $0.2\text{-}\mu\text{m}$ Gelman HT-200 polysulfone membrane, which allowed porewater sampling from about 23–25 cm below the sediment-water interface (SWI) to 5 cm above this interface (thereafter referred to as overlying water) at a 1-cm depth resolution. Oxygen was removed from the peepers prior to their deployment, as described by Laforte et al. (2005). Four peepers were left in the sediments of each lake basin for at least 15 d, i.e., a longer time period than that required for solute concentrations in the peeper cells to reach equilibrium with those in the porewater (5–
95 10 d; Hesslein, 1976; Carignan et al., 1985). At least three independent porewater profiles of pH, of the concentrations of CH_4 , DIC, acetate, NO_3^- , SO_4^{2-} , Fe and Mn, and of the $\delta^{13}\text{C}$ of CH_4 and DIC were generated for the two sampling sites. In Lake



Bédard, samples were also collected to determine three porewater profiles of sulfide concentrations ($\Sigma\text{S}(-\text{II})$). After peeper retrieval, samples (0.9–1.9 mL) for CH_4 and DIC concentrations and $\delta^{13}\text{C}$ measurements were collected within 5 minutes from the peeper cells with He-purged polypropylene syringes. They were injected through rubber septa into He-purged 3.85-mL exetainers (Labco Limited), after removal of a volume equivalent to that of the collected porewater. The exetainers were preacidified with 40–80 μL of HCl 1N to reach a final $\text{pH} \leq 2$. The protocols used to collect and preserve water samples for the other solutes are given by Laforte et al. (2005).

2.2 Analyses

Concentrations and carbon isotopic composition of CH_4 and DIC were measured as described by Clayer et al. (2018). Briefly, the concentrations were analyzed within 24 h of peeper retrieval by gas chromatography with a precision better than 4 % and detection limits (DL) of 2 μM and 10 μM for CH_4 and DIC, respectively. The $^{13}\text{C}/^{12}\text{C}$ abundance ratios of CH_4 and CO_2 were determined by Mass Spectrometry with a precision of ± 0.2 ‰ when 25 μmol of an equimolar mixture of CH_4 and CO_2 was injected, and results are reported as:

$$\delta^{13}\text{C} = 1000 \left(\frac{\left(\frac{^{13}\text{C}_{\text{solute}}}{^{12}\text{C}_{\text{solute}}} \right)_{\text{sample}}}{\left(\frac{^{13}\text{C}}{^{12}\text{C}} \right)_{\text{standard}}} - 1 \right) \quad (1)$$

where the subscript solute stands for CH_4 or DIC and the reference standard is Vienna Pee Dee Belemnite (VPDB). Acetate concentration was determined by ion chromatography (DL of 1.4 μM) and those of Fe, Mn, NO_3^- , SO_4^{2-} and $\Sigma\text{S}(-\text{II})$, as given by Laforte et al. (2005).

2.3 Modeling of porewater solutes and the reaction network

The computer program WHAM 6 (Tipping, 2002) was used, as described by Clayer et al. (2016), to calculate the speciation of porewater cations and anions. The solute activities thus obtained, together with solubility products (K_s), were used to calculate saturation index values ($\text{SI} = \log \text{IAP}/K_s$, where IAP is the ion activity product).

The following one-dimensional mass-conservation equation (Boudreau, 1997):

$$\frac{\partial}{\partial x} \left(\varphi D_s \frac{\partial [\text{solute}]}{\partial x} \right) + \varphi \alpha_{\text{irrigation}} ([\text{solute}]_{\text{tube}} - [\text{solute}]) + R_{\text{net}}^{\text{solute}} = 0 \quad (2)$$

was used to model the porewater profiles of CH_4 , DIC, O_2 , Fe and SO_4^{2-} , assuming steady state and negligible solute transport by bioturbation and advection (Clayer et al., 2016). In this equation, $[\text{solute}]$ and $[\text{solute}]_{\text{tube}}$ denote a solute concentration in the porewater and in the animal tubes (assumed to be identical to that in the overlying water), respectively, x is depth (positive downward), φ is porosity, D_s is the solute effective diffusion coefficient in sediments, $\alpha_{\text{irrigation}}$ is the bioirrigation coefficient, and $R_{\text{net}}^{\text{solute}}$ (in mol cm^{-3} of wet sediment s^{-1}) is the solute net production rate (or consumption rate if $R_{\text{net}}^{\text{solute}}$ is negative). D_s was assumed to be $\varphi^2 D_w$ (Ullman and Aller, 1982), where D_w is the solute tracer diffusion coefficient in water.



The values of D_w , corrected for in situ temperature (Clayer et al., 2018), were $9.5 \times 10^{-6} \text{ cm}^2 \text{ s}^{-1}$, $6.01 \times 10^{-6} \text{ cm}^2 \text{ s}^{-1}$ and $1.12 \times 10^{-5} \text{ cm}^2 \text{ s}^{-1}$ for CH_4 , HCO_3^- and CO_2 , respectively. The values of $\alpha_{\text{irrigation}}$ in Lake Tantaré Basin A were calculated as in
125 Clayer et al. (2016), based on an inventory of benthic animals (Hare et al., 1994), and were assumed to be 0 in Lake Bédard since its bottom water was anoxic (Fig. 1).

The $R_{\text{net}}^{\text{solute}}$ values were determined from the average ($n = 3$ or 4) solute concentration profiles by numerically solving Eq. (2) with the computer code PROFILE (Berg et al., 1998). The boundary conditions were the solute concentrations at the top and at the base of the porewater profiles. In situ porewater O_2 profiles were not measured in Lake Tantaré Basin A. For modeling
130 this solute with PROFILE, we assumed that the $[\text{O}_2]$ in the overlying water was identical to that measured in the lake bottom water and equal to 0 below 0.5 cm (based on O_2 penetration depth; Couture et al., 2016). This procedure provides a rough estimate of $R_{\text{net}}^{\text{O}_2}$ at the same vertical resolution as for the other solutes. The code PROFILE yields a discontinuous profile of discrete $R_{\text{net}}^{\text{solute}}$ values over depth intervals (zones) which are objectively selected by using the least square criterion and statistical F-testing (Berg et al., 1998). The fluxes of solute transport across the SWI due to diffusion and bioirrigation are also
135 estimated by PROFILE. In order to estimate the variability in $R_{\text{net}}^{\text{solute}}$ related to heterogeneity within the 25-m^2 sampling area, additional $R_{\text{net}}^{\text{solute}}$ values were obtained by modeling the average profiles whose values were increased or decreased by one standard deviation. This variability generally ranges between 2 and $10 \text{ fmol cm}^{-3} \text{ s}^{-1}$.

The main reactions retained in this study to describe carbon cycling in the sediments of the two lake basins are shown in Table 1. Once oxidants are depleted, fermentation of metabolizable OM (r1) can yield acetate, CO_2 and H_2 . The partial degradation
140 of high molecular weight OM (HMW OM) into lower molecular weight OM (LMW OM) can also produce CO_2 (r2, Corbett et al., 2013; Corbett et al., 2015). Acetoclasty (r3) and hydrogenotrophy (r4) yield CH_4 . Moreover, CH_4 (r5) and OM (r6) can be oxidized to CO_2 when electron acceptors such as O_2 , Fe(III) and SO_4^{2-} are present. Note that the electron acceptors (EAs) NO_3^- and Mn oxyhydroxides can be neglected in these two lake basins (Feyte et al., 2012; Clayer et al., 2016) as well as the precipitation of metal carbonates whose saturation index values are negative ($\text{SI} \leq -1.5$) except for siderite (r7) in Lake Bédard
145 ($\text{SI} = 0.0$ to 0.7). Lastly, sulfide oxidation by iron oxides (r8), which can be a source of SO_4^{2-} and H_2 (Holmkvist et al., 2011; Clayer et al., 2018), is also considered.

From Table 1, the net rate of CH_4 production, $R_{\text{net}}^{\text{CH}_4}$, in the sediments is:

$$R_{\text{net}}^{\text{CH}_4} = R_3 + R_4 - R_5 \quad (3)$$

where R_3 and R_4 are the rates of acetoclastic (r3) and hydrogenotrophic (r4) production of CH_4 , respectively, and R_5 is the rate of DIC production due to CH_4 oxidation (r5). The net rate of DIC production, $R_{\text{net}}^{\text{DIC}}$, can be expressed as:

$$R_{\text{net}}^{\text{DIC}} = R_1 + R_2 + R_3 - R_4 + R_5 + R_6 - R_7 \quad (4)$$

150 where R_1 , R_2 and R_6 are the rates of DIC production due to complete fermentation of labile OM (r1), partial fermentation of HMW OM (r2) and OM oxidation (r6), respectively, and R_7 is the rate of DIC removal by siderite precipitation (r7). It can also be written that:



$$R_{\text{net}}^{\text{Ox}} = -2R_5 - R_6 \quad (5)$$

where $R_{\text{net}}^{\text{Ox}}$ is the net reaction rate of all the oxidants (O_2 , Fe(III) and SO_4^{2-}) consumption. For simplicity, $R_{\text{net}}^{\text{Ox}}$ is expressed in equivalent moles of O_2 consumption rate, taking into account that SO_4^{2-} and Fe(III) have twice and one quarter the oxidizing capacity of O_2 , respectively. In practice, the value of $R_{\text{net}}^{\text{Ox}}$ was calculated by adding those of $R_{\text{net}}^{\text{O}_2}$, $\frac{1}{4}R_{\text{net}}^{\text{Fe(III)}}$ and $2R_{\text{net}}^{\text{SO}_4^{2-}}$ where $R_{\text{net}}^{\text{O}_2}$, $R_{\text{net}}^{\text{Fe(III)}}$ and $R_{\text{net}}^{\text{SO}_4^{2-}}$ were estimated with PROFILE. In this calculation, we assumed that all dissolved Fe is in the form of Fe(II), and that the rate of Fe(II) consumption through reactions r7 is negligible compared to those associated with reactions r5 and r6. Under these conditions, $R_{\text{net}}^{\text{Fe(III)}} = -R_{\text{net}}^{\text{Fe}}$.

2.4 Modeling of the $\delta^{13}\text{C}$ profiles

The $\delta^{13}\text{C}$ profiles of CH_4 ($\delta^{13}\text{C}\text{-CH}_4$) and DIC ($\delta^{13}\text{C}\text{-DIC}$) were simulated with a modified version of Eq. 1 (Clayer et al., 2018):

$$\delta^{13}\text{C} = 1000 \left(\frac{\left(\frac{[^{13}\text{C}]}{[\text{C}]} \right)_{\text{sample}}}{\left(\frac{^{13}\text{C}}{^{12}\text{C}} \right)_{\text{standard}}} - 1 \right) \quad (6)$$

where $[\text{C}]$ is the total CH_4 or DIC concentration ($[^{12}\text{C}]$ can be replaced by $[\text{C}]$ since $\sim 99\%$ of C is ^{12}C), and $[^{13}\text{C}]$ is the isotopically heavy CH_4 or DIC concentration. Equation 6 allows calculating a $\delta^{13}\text{C}$ profile once the depth distributions of $[^{13}\text{C}]$ and $[\text{C}]$ are known. This information is obtained by solving the mass-conservation equations of C and ^{13}C for CH_4 and DIC. The one-dimensional mass-conservation of $[\text{C}]$ is given by Eq. 2 where [solute] is replaced by $[\text{C}]$, whereas that for $[^{13}\text{C}]$ is the following modified version of Eq. 2 (Clayer et al., 2018):

$$\frac{\partial}{\partial x} \left(\varphi \frac{D_s}{f} \frac{\partial [^{13}\text{C}]}{\partial x} \right) + \varphi \alpha_{\text{Irrigation}} ([^{13}\text{C}]_{\text{tube}} - [^{13}\text{C}]) + \sum_{i=1}^5 \frac{R_i}{\alpha_i} \left(\frac{\delta^{13}\text{C}_i^{\text{reactant}}}{1000} + 1 \right) \left(\frac{^{13}\text{C}}{^{12}\text{C}} \right)_{\text{standard}} = 0 \quad (7)$$

where f , the molecular diffusivity ratio, is the diffusion coefficient of the regular solute divided by that of the isotopically heavy solute, α_i is the isotope fractionation factor in reaction r_i , and $\delta^{13}\text{C}_i^{\text{reactant}}$ is the $\delta^{13}\text{C}$ of the reactant leading to the formation of the solute (CH_4 or DIC) in reaction r_i . Input and boundary conditions used to numerically solve Eqs 2 and 7 for $[\text{C}]$ and $[^{13}\text{C}]$, respectively, via the `bvp5c` function of MATLAB[®] are described in section 3.4 and in section S2 of the Supporting Information (SI).

The goodness of fit of the model was assessed with the norm of residuals (N_{res}):

$$N_{\text{res}} = \sqrt{\sum_{x=0.5}^{22.5} (\delta^{13}\text{C}_m - \delta^{13}\text{C}_s)^2} \quad (8)$$



where $\delta^{13}\text{C}_m$ and $\delta^{13}\text{C}_s$ are the measured and simulated $\delta^{13}\text{C}$ values, respectively. The norm of residuals (N_{res}) varies between 0 and infinity with smaller numbers indicating better fits.

175 2.5 Data treatment of other data sets

To better assess the COS of the fermenting OM in lakes, relevant sets of porewater concentration profiles (CH_4 , DIC, EAs, Ca) available from the literature or from our data repository have been modeled with the code PROFILE, as described in section 2.3, to extract their $R_{\text{net}}^{\text{CH}_4}$, $R_{\text{net}}^{\text{DIC}}$ and $R_{\text{net}}^{\text{Ox}}$ profiles. These porewater datasets, described in section S3 of the SI, had been generated by sampling porewater in the hypolimnetic sediments of: i) Lake Bédard and Basin A of Lake Tantaré, at other dates
180 than for this study (Clayer et al, 2016); ii) Basin B of Lake Tantaré (adjacent to Basin A; Fig 1), on four occasions (Clayer et al., 2016; 2018); iii) Williams Bay of Jacks Lake ($44^{\circ}41' \text{ N}$, $78^{\circ}02' \text{ W}$), located in Ontario, Canada, on the edge of the Canadian Shield (Carignan and Lean 1991); iv) the southern basin of the alpine Lake Lugano ($46^{\circ}00' \text{ N}$, $3^{\circ}30' \text{ E}$) located in Switzerland, on two occasions (Lazzaretti-Ulmer and Hanselmann 1999). All lake basins, except Basin A of Lake Tantaré develop an anoxic hypolimnion.

185 3 Results

3.1 Solute concentration profiles

Differences among the replicate profiles of CH_4 , DIC, SO_4^{2-} , $\Sigma\text{S}(-\text{II})$ and Fe (Fig. 2) at the two sampling sites are generally small (except perhaps those of SO_4^{2-} in Lake Bédard) and should be mainly ascribed to spatial variability within the 25- m^2 sampling area. Indeed, the main vertical variations in the profiles are defined by several data points without the sharp
190 discontinuities expected from sampling and handling artifacts. Note that the acetate concentrations, which were consistently low ($< 2 \mu\text{M}$), are not shown.

The low Fe ($< 5 \mu\text{M}$; Fig. 2f) and CH_4 ($< 2 \mu\text{M}$; Fig. 2a) concentrations as well as the relatively high SO_4^{2-} concentrations ($36 \pm 2.1 \mu\text{M}$; Fig. 2e) in the sediment overlying water of Lake Tantaré Basin A are all consistent with the $[\text{O}_2]$ ($\sim 2.5 \text{ mg L}^{-1}$) measured in the bottom water and are indicative of oxic conditions at the sediment surface. The sharp Fe gradients near the
195 SWI indicate an intense recycling of Fe oxyhydroxides (Fig. 2f; Clayer et al., 2016) and the concave-down curvatures in the SO_4^{2-} profiles (Fig. 2e) reveal SO_4^{2-} reduction near the SWI. In contrast to Lake Tantaré Basin A, high Fe ($> 200 \mu\text{M}$), measurable CH_4 ($> 200 \mu\text{M}$) low SO_4^{2-} ($2.7 \pm 1.4 \mu\text{M}$) and detectable $\Sigma\text{S}(-\text{II})$ concentrations in the overlying waters of Lake Bédard (Fig. 2i, m and n) are consistent with anoxic conditions at the sediment surface. The absence of a sharp Fe gradient at the SWI in Lake Bédard suggests that Fe oxyhydroxides were not recycled in these sediments when porewater sampling
200 occurred.

In the two lake basins, SO_4^{2-} concentrations reach a minimum between the SWI and 5 cm depth (Fig. 2e and m), and increase below these depths. Alongside, all Fe profiles show a slight increase downward (Fig. 2f and n) indicating that solid Fe(III) is



reduced to produce dissolved Fe. In Lake Bédard, the $\Sigma S(-II)$ concentrations decrease from the SWI to ~ 10 cm depth and remain relatively constant below that depth at $0.08 \pm 0.06 \mu\text{M}$ for two of the profiles and at $0.71 \pm 0.18 \mu\text{M}$ for the other one
205 (grey filled triangles in Fig. 2n).

The concentrations of CH_4 (< 1.5 mM; Fig. 2a and i) are well below saturation at 4°C and *in situ* pressure (4.4–5.5 mM; Duan and Mao, 2006), implying that CH_4 ebullition is a negligible CH_4 transport process. The CH_4 values increases from $< 2 \mu\text{M}$ in the overlying water to 0.18–0.20 mM at the base of the Lake Tantaré Basin A profiles (Fig. 2a), and from 0.2–0.5 mM to 1.0–1.4 mM in those of Lake Bédard (Fig. 2i). The three CH_4 profiles from Lake Tantaré Basin A (Fig. 2a) show a modest concave-up curvature in their upper part, close to the SWI, indicative of a net CH_4 consumption, and a convex-up curvature in their
210 up curvature in their upper part, close to the SWI, indicative of a net CH_4 consumption, and a convex-up curvature in their lower part, typical of a net CH_4 production. Such trends, however, are not observed in Lake Bédard sediments. The CH_4 profiles from this lake exhibit a convex-up curvature over the whole sediment column, although more pronounced in its upper part (Fig. 2i).

The DIC concentrations consistently increase from 0.27–0.32 mM and 1.2–1.5 mM in the sediment overlying water to 0.76–
215 0.83 mM and 3.5–4.3 mM at the bottom of the profiles in Lake Tantaré Basin A and Lake Bédard, respectively (Fig. 2c and k). All DIC profiles show a similar shape with a slight concave-up curvature in their lower segment and a convex-up curvature in their upper portions.

3.2 Modeled CH_4 and DIC concentration profiles

The modeled $[\text{CH}_4]$ and DIC profiles accurately fit the average ($n = 3$ or 4) data points ($r^2 > 0.996$ and $r^2 > 0.998$ for CH_4 and
220 DIC, respectively; Fig. 2g,h,o and p). The $R_{\text{net}}^{\text{CH}_4}$ profiles reveal three zones in each lake basin numbered Z_1 , Z_2 and Z_3 from the sediment surface whose boundaries match those defined by the $R_{\text{net}}^{\text{DIC}}$ profiles. For Lake Tantaré Basin A, Z_1 corresponds to a net CH_4 consumption and Z_2 and Z_3 to net CH_4 production, with the highest rate in Z_2 (Fig. 2g). In contrast, the three zones in Lake Bédard show net CH_4 production with the highest rate in Z_1 and the lowest in Z_3 (Fig. 2o). The $R_{\text{net}}^{\text{DIC}}$ profiles in both lake basins show a zone of net DIC consumption below two zones of net DIC production with the highest rate values in the Z_1 and
225 Z_2 for Lake Tantaré Basin A and Lake Bédard, respectively.

The $R_{\text{net}}^{\text{CH}_4}$ and $R_{\text{net}}^{\text{DIC}}$ profiles displayed in Figure 2 are, among all the possible solutions, the ones that give the simplest rate profile while providing a satisfying explanation of the averaged solute concentration profile as determined by statistical F-testing implemented in the code PROFILE (P value ≤ 0.001 except for the $R_{\text{net}}^{\text{DIC}}$ profile in Lake Bédard whose P value is ≤ 0.005). As an additional check of the robustness of the depth distribution of $R_{\text{net}}^{\text{CH}_4}$ and $R_{\text{net}}^{\text{DIC}}$ provided by PROFILE, we used
230 another inverse model, i.e., Rate Estimation from Concentrations (REC; Lettmann et al., 2012) to model the average CH_4 and DIC profiles. Note that the statistical method, implemented in REC to objectively select the depth distribution of the net reaction rates, i.e., the Tikhonov regularization technique, differs from that of PROFILE. Figure S1 (SI) shows that the two codes predicted mutually consistent $R_{\text{net}}^{\text{CH}_4}$ and $R_{\text{net}}^{\text{DIC}}$ profiles, with rate values of similar magnitude. PROFILE was also used in this study to estimate $R_{\text{net}}^{\text{SO}_4^{2-}}$, $R_{\text{net}}^{\text{Fe}}$ and $R_{\text{net}}^{\text{O}_2}$ in order to calculate the value of $R_{\text{net}}^{\text{Ox}}$ in each zone at both sampling sites (see



235 section 2.3 for details). The modeled $[\text{SO}_4^{2-}]$ and $[\text{Fe}]$ profiles are not shown but, again, they accurately fit the data points ($r^2 > 0.983$). As expected from the contrasting O_2 regimes of the two lake basins, $R_{\text{net}}^{\text{Ox}}$ values for Lake Tantaré Basin A were one to two orders of magnitude higher than those for Lake Bédard. Note that $R_{\text{net}}^{\text{O}_2}$ was by far the highest contributor to the value of $R_{\text{net}}^{\text{Ox}}$ in Lake Tantaré Basin A with values of -290 and $-72 \text{ fmol cm}^{-3} \text{ s}^{-1}$ in the Z_1 and Z_2 , respectively. The values of $R_{\text{net}}^{\text{CH}_4}$, $R_{\text{net}}^{\text{DIC}}$ and $R_{\text{net}}^{\text{Ox}}$ estimated in each zone of each lake basins are reported in Table 2.

240 3.3 The $\delta^{13}\text{C}$ profiles

The $\delta^{13}\text{C}$ -DIC values increase from $-28.2 \pm 0.4 \text{ ‰}$ and $-17.2 \pm 0.7 \text{ ‰}$ in the overlying water to $-5.1 \pm 1.0 \text{ ‰}$ and $3.6 \pm 1.7 \text{ ‰}$ at the base of the profiles in Lake Tantaré Basin A and Lake Bédard, respectively (Fig. 2d and l). Similarly, the $\delta^{13}\text{C}$ - CH_4 values in Lake Bédard increase steadily from $-82.5 \pm 3.3 \text{ ‰}$ in the overlying water to $-74.0 \pm 1.5 \text{ ‰}$ at 24.5 cm depth (Fig. 2j). Regarding Lake Tantaré Basin A, the CH_4 concentrations above 1.5 cm depth were too low for their $^{13}\text{C}/^{12}\text{C}$ ratio to be
245 determined. Starting at 1.5 cm depth, the $\delta^{13}\text{C}$ - CH_4 values first decrease from $-91.1 \pm 11.1 \text{ ‰}$ to $-107.0 \pm 6.8 \text{ ‰}$ at 2.5 cm depth and then increase progressively to $-83.5 \pm 1.6 \text{ ‰}$ at the base of the profiles (Fig. 2b). Note that a shift toward more positive $\delta^{13}\text{C}$ - CH_4 values upward, generally attributed to the oxidation of CH_4 (Chanton et al., 1997; Norđi et al., 2013), is only observed in the profiles of Lake Tantaré Basin A (Fig. 2b).

As shown in Fig. S2 (SI), the isotopic signatures of nearly all samples from the two lake basins fall within the ranges reported
250 for hydrogenotrophic methanogenesis, i.e., CO_2 reduction, in a $\delta^{13}\text{C}$ - CO_2 vs $\delta^{13}\text{C}$ - CH_4 graph similar to that proposed by Whiticar (1999). Indeed, the values of $\delta^{13}\text{C}$ - CH_4 which are lower than -70 ‰ over the whole profiles in the two lake basins, and the large difference (67 to 92 ‰) between the $\delta^{13}\text{C}$ of gaseous CO_2 ($\delta^{13}\text{C}$ - CO_2) and $\delta^{13}\text{C}$ - CH_4 , strongly contrast with the typical $\delta^{13}\text{C}$ - CH_4 values (-68 to -50 ‰) and with the difference between $\delta^{13}\text{C}$ - CO_2 and $\delta^{13}\text{C}$ - CH_4 (39 to 58 ‰) reported for acetoclasty (Whiticar, 1999). The $\delta^{13}\text{C}$ results reported previously for another basin of Lake Tantaré (Basin B; Clayer et al.,
255 2018) show also in the hydrogenotrophy domain in Fig. S2.

3.4 Modeled $\delta^{13}\text{C}$ profiles

In order to model the $\delta^{13}\text{C}$ profiles with Eq. 6, accurate profiles of $[\text{C}]$ and $[\text{C}]^{13}$ need first to be determined by numerically solving Eqs. 2 and 7, respectively. The modeled profiles of $[\text{CH}_4]$ and DIC obtained with Eq. 2 replicated well the measured profiles of these two solutes when the depth distributions of $R_{\text{net}}^{\text{CH}_4}$ or $R_{\text{net}}^{\text{DIC}}$ provided by PROFILE (Table 2) and those of D_s ,
260 $\alpha_{\text{irrigation}}$ and ϕ were used as inputs in Eq. 2, and when measured CH_4 or DIC concentrations at the top and bottom of the profiles were imposed as boundary conditions. Getting a truthful profile of $[\text{C}]^{13}$ with Eq. 7 requires, however, accurate values of $\delta^{13}\text{C}_i^{\text{reactant}}$, α_i , and R_i for each of the reactions given in Table 1, and of f for both CH_4 (f - CH_4) and DIC (f -DIC). The multi-step procedure followed to obtain the best $[\text{C}]^{13}$ profiles for CH_4 and DIC is described in section S2 (SI). This modeling exercise revealed that $R_3 = 0$ for all the zones in the sediments of both lake basins, thus confirming that practically all CH_4 is
265 produced through hydrogenotrophy, as inferred above from the $\delta^{13}\text{C}$ values.

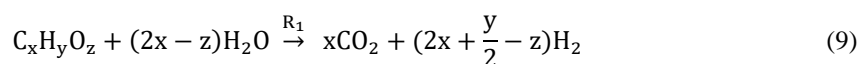


The best fits between the simulated and measured $\delta^{13}\text{C}$ profiles of CH_4 and DIC for Lake Tantaré Basin A and Lake Bédard (red lines in Fig. 3) were obtained with the f , α_i and R_i values displayed in Table 3. The optimal α_i and f values were within the ranges reported in the literature for both lake basins, except for the lower-than-expected value of α_2 (0.984) in the Z_2 of Lake Bédard. Note that α_3 is not given in Table 3 since the modeling of the $\delta^{13}\text{C}$ profiles of CH_4 and DIC indicates that $R_3 = 0$ (see section S2.2.2.1 in the SI). Optimal values for α_4 , α_5 and $f\text{-CH}_4$ for both lake basins were also similar to those reported in our previous study on Lake Tantaré Basin B (Clayer et al., 2018).

4 Discussion

4.1 Organic matter mineralization pathways at the sampling sites

The porewater data as well as the combined modeling of carbon isotopes and concentration profiles, allows to highlight key OM mineralization mechanisms and to quantify the relative contribution of methanogenesis and fermentation to OM degradation at both sampling sites. The ^{13}C isotopic signatures, i.e., highly negative values of $\delta^{13}\text{C}\text{-CH}_4$ and large differences between $\delta^{13}\text{C}\text{-CO}_2$ and $\delta^{13}\text{C}\text{-CH}_4$ (section 3.3 and Fig. S2 in the SI), as well as the modeling of the $\delta^{13}\text{C}\text{-CO}_2$ and $\delta^{13}\text{C}\text{-CH}_4$ profiles (section S2.2.2.1 and Fig S4a and b in the SI) all point to hydrogenotrophy as being the only pathway for methanogenesis in the two lake basins. The dominance of hydrogenotrophy is consistent also with the finding that acetate concentrations were close to or below DL in the porewater samples. Under the condition that acetoclasty is negligible (i.e., $x = \nu_1$), reaction r1 from Table 1 becomes:



Methanogenesis was also reported to be essentially hydrogenotrophic in the sediments of Basin B of Lake Tantaré (Clayer et al 2018). The absence of acetoclasty in the sediments of the oligotrophic lakes Bédard and Tantaré is consistent with the consensus that hydrogenotrophy becomes an increasingly important CH_4 production pathway: i) when labile OM is depleted (Whiticar et al., 1986; Chasar et al., 2000; Hornibrook et al., 2000), ii) with increasing sediment/soil depth (Hornibrook et al., 1997; Conrad et al., 2009), or iii) with decreasing rates of primary production in aquatic environments (Wand et al., 2006; Galand et al., 2010).

The modelling of concentrations and $\delta^{13}\text{C}$ profiles revealed that oxidative processes occurred essentially in the upper 7 cm of the sediments of the perennially oxygenated Lake Tantaré Basin A, i.e., mainly in the Z_1 and, to a lesser extent, in the Z_2 (Table 3 and sections S2.1.2.1 and S2.1.2.2 of the SI). Moreover, it showed that methanotrophy was the dominant oxidative reaction in these sediment layers since 75% of the oxidants were consumed through r5 (section S2.2.2.2 of the SI). This outcome is consistent with several studies showing that methanotrophy occurs at higher rates than OM oxidation at low EA concentrations (Sivan et al., 2007; Pohlman et al., 2013; Kankaala et al., 2013; Thottahil et al., 2019). Methanotrophy is also evidenced in the Z_1 of this lake basin by the negative $R_{\text{net}}^{\text{CH}_4}$ value and by a shift of the $\delta^{13}\text{C}\text{-CH}_4$ profiles to more positive values in their upper part (Fig. 2b and g). Use of Eq. 2 to model the EAs profiles with the code PROFILE predicts that O_2 was by far the main EA



involved either directly, or indirectly via the coupling with the Fe or S cycles, in the oxidative processes. Indeed, comparing the values of $R_{\text{net}}^{\text{O}_2}$ and $R_{\text{net}}^{\text{Ox}}$ (see Section 3.2 and Table 2) shows that O_2 accounts for 87% and 70% of the oxidants consumed in the Z_1 and Z_2 of Lake Tantaré Basin A, respectively. Since O_2 penetration in the sediment by molecular diffusion is limited to ~4-mm, a significant amount of O_2 is predicted by Eq. 2 to be transported deeper in the sediment through bioirrigation. The
300 predominance of O_2 among the EAs consumed in the sediments is consistent with our previous study in this basin of Lake Tantaré (Clayer et al., 2016). Given that methanotrophy is the dominant oxidative process and that O_2 is the main oxidant consumed, it is probable that aerobic oxidation of methane prevails over its anaerobic counterpart in this lake basin. This is in line with the common thinking that CH_4 oxidation in freshwater lake sediments is carried out by methanotrophs essentially in the uppermost oxic sediment layer (Bastviken et al., 2008 and references therein).

305 The sharp upward depletion in $^{13}\text{C}\text{-CH}_4$ leading to a minimum $\delta^{13}\text{C}\text{-CH}_4$ value at 2.5 cm depth in Lake Tantaré Basin A sediments (Fig. 3a) was unanticipated since, according to the modeling with the code PROFILE, it occurs in the methanotrophic zone, i.e., where the remaining CH_4 is expected to be ^{13}C -enriched as a result of CH_4 oxidation. Marked $^{13}\text{C}\text{-CH}_4$ depletions at the base of the sulfate-methane transition zone, where CH_4 is consumed via SO_4^{2-} reduction, have often been observed in marine sediments (Burdige et al., 2016 and references therein). Such features are generally attributed to the production of CH_4
310 by hydrogenotrophy from the ^{13}C -depleted DIC resulting from the anaerobic CH_4 oxidation, a process referred to as intertwined methanotrophy and hydrogenotrophy (e.g., Borowski et al., 1997; Pohlman et al., 2008; Burdige et al., 2016). Here the modelled $\delta^{13}\text{C}\text{-CH}_4$ profile captured the minimum in $\delta^{13}\text{C}\text{-CH}_4$ in the Z_1 by simply assuming concomitant hydrogenotrophy and methanotrophy in this zone and an upward-increasing α_4 value from 1.085 in the Z_3 to 1.094 in the Z_1 (section S2.2.1 of the SI). These α_4 values remain within the range reported for this isotope fractionation factor (Table S1 in the SI). A small
315 variation with sediment depth in the fractionation factor α_4 is arguably possible since its value depends on the types of microorganisms producing CH_4 (Conrad 2005). The possibility that a depth variation in this isotope fractionation factor could explain some of the minima in $\delta^{13}\text{C}\text{-CH}_4$ reported in other studies should be considered.

In the Z_2 of Lake Bédard, the net rate of DIC production (i.e., $167 \text{ fmol cm}^{-3} \text{ s}^{-1}$) was more than 3 times that of CH_4 production ($50 \text{ fmol cm}^{-3} \text{ s}^{-1}$; Table 2). Given that the $R_{\text{net}}^{\text{Ox}}$ was negligible in this zone (i.e., $R_5 = R_6 = 0$), we obtain from Eqs 3 and 4 and
320 Table 2 that $R_{\text{net}}^{\text{CH}_4} = R_4 = 50 \text{ fmol cm}^{-3} \text{ s}^{-1}$ and $R_{\text{net}}^{\text{DIC}} = R_1 + R_2 - R_4 = 167 \text{ fmol cm}^{-3} \text{ s}^{-1}$ (see section S2.1.2.2 of the SI). Should we assume that DIC production by r2 is negligible, i.e., $R_2 = 0$, a R_1/R_4 ratio of 4.3 would be obtained. This high ratio indicates that DIC was not produced by hydrogenotrophy (r4) coupled to fermentation (r1) alone in the Z_2 of this lake. Indeed, methanogenesis through the coupling of these two reactions yields a R_1/R_4 ratio of 2 if the fermenting substrate is carbohydrates (COS of 0) and lower than 2 if the fermenting substrate has a negative COS value. We thus attributed the
325 production of the additional DIC to the partial fermentation of HMW OM, an assumed non-fractionating process reported to occur in wetlands (Corbett et al., 2015). The better fitting of the $\delta^{13}\text{C}\text{-DIC}$ profile when α_2 is set to 0.980–0.984 rather than to 1.000 in the Z_2 (compare the blue and red lines in Fig. 4b) suggests that C fractionates during this partial fermentation process. Table 3 displays the depth-integrated reaction rates (ΣR_i) over the top 21cm of the sediment column which are given by:



$$\Sigma R_i = \sum_{j=1}^3 \Delta x_j R_i \quad (10)$$

where Δx_j (cm) is the thickness of the zone Z_j . In this calculation, we assume that other zones of CH_4 or DIC production are
absent below 21 cm. Values of ΣR_i clearly show that anaerobic carbon mineralization reactions (fermentation and
methanogenesis) are important contributors to the overall OM mineralization in the two studied lake basins. Indeed, the sum
of the rates of CH_4 production (ΣR_4), DIC production due to CH_4 formation ($\Sigma R_1 - \Sigma R_4$) and HMW OM partial fermentation
(ΣR_2) represents 49% and 100% of the total OM degradation rate ($\Sigma R_1 + \Sigma R_2 + \Sigma R_5 + \Sigma R_6$) in the sediment of lakes Tantaré
Basin A and Bédard, respectively. The contribution of anaerobic mineralization for Lake Tantaré Basin A is about 1.6 times
higher than the average of 30% reported for this lake basin in a previous study (Clayer et al., 2016). This significant discrepancy
arises because these authors, in the absence of isotopic data to adequately constrain the R_i values, assumed that $R_4 = 0$ in the
net methanotrophic zone Z_1 . Should we make the same assumption in the present study, we would also estimate that
fermentation and methanogenesis represent only 30% of the total rate of OM degradation in the oxygenated Lake Tantaré
Basin A and we would thus underestimate the importance of methanogenesis. The inclusion of $\delta^{13}\text{C}$ data in the present
modeling study thus allowed to better constrain the effective rates of CH_4 production (R_4).

4.2 Organic substrates for methanogenesis at the sampling sites

Table 3 indicates that hydrogenotrophy (r_4) coupled to the complete fermentation of OM (r_1) produces CH_4 at higher rates
(R_4) than DIC ($R_1 - R_4$) in the Z_1 and Z_2 of both lake basins. This outcome is inconsistent with the equimolar production of
 CH_4 and DIC expected from the fermentation of glucose ($\text{C}_6\text{H}_{12}\text{O}_6$), the model molecule used to represent labile OM in
diagenetic models (Paraska et al., 2014), thus suggesting that the fermentation of this compound is not the exclusive source of
the H_2 required for hydrogenotrophy. Had OM been represented by $\text{C}_6\text{H}_{12}\text{O}_6$ in r_1 , the rate of H_2 production by this reaction
would have been twice that of CO_2 , i.e., $2R_1$. For its part, the rate of H_2 consumption through hydrogenotrophy is four times
that of the CH_4 production, i.e., $4R_4$. Hence, an additional H_2 production at rates of up to 212 and 70 $\text{fmol cm}^{-3} \text{ s}^{-1}$, i.e., $4R_4 -$
 $2R_1$, is needed to balance the H_2 production rate expected from the fermentation of $\text{C}_6\text{H}_{12}\text{O}_6$ and the H_2 consumption rate by
hydrogenotrophy observed in the sediments of Lake Tantaré Basin A and Lake Bédard, respectively. As discussed by Clayer
et al. (2018), this additional production rate of H_2 could be provided by a cryptic Fe-S cycle such as r_8 (Table 1), or by the
production of CH_4 via the fermentation of organic substrates more reduced than glucose.

The progressive downward increases in dissolved Fe and SO_4^{2-} (Fig. 2e, f, m and n) below ~ 5 cm depth and decrease in $\Sigma\text{S}(-\text{II})$
(Fig. 2n) observed in the porewaters support a production of H_2 from r_8 in both lakes. However, modeling the appropriate
solute profiles with the code PROFILE indicates that the production rates of dissolved Fe ($< 10 \text{ fmol cm}^{-3} \text{ s}^{-1}$) and SO_4^{2-} (< 1
 $\text{fmol cm}^{-3} \text{ s}^{-1}$) and the consumption rate of $\Sigma\text{S}(-\text{II})$ ($< 1 \text{ fmol cm}^{-3} \text{ s}^{-1}$) are about one order of magnitude too low to explain the
missing H_2 production rate in both basins. Moreover, in the Z_1 and Z_2 of Lake Tantaré Basin A, the rate of solid Fe(III)
reduction ($< 3 \text{ fmol cm}^{-3} \text{ s}^{-1}$; calculated from Liu et al. 2015) is much lower than that required from r_8 (i.e., 1 to 2 times the



360 additional H₂ production of $4R_4 - 2R_1$; $70\text{--}424 \text{ fmol cm}^{-3} \text{ s}^{-1}$) to produce sufficient amounts of H₂ to sustain the additional hydrogenotrophy. Given these results, we submit that a cryptic Fe-S cycle, if present, would contribute only minimally to the missing rate of H₂ production, and that the fermentation of reduced organic compounds could provide a better explanation to the imbalance between the H₂ production and consumption rates.

Since CH₄ is produced by hydrogenotrophy in the two lake basins ($\chi_H = 1$), Eqn. S15 (section S2.2.2. of the SI) describing the COS of the fermenting organic substrate C_xH_yO_z simplifies as:

$$\text{COS} = -4 \left(\frac{2 \left(R_{\text{net}}^{\text{CH}_4} - \frac{1}{2} \chi_M R_{\text{net}}^{\text{Ox}} \right) - R_1}{R_1} \right) \quad (11)$$

365 where χ_M is the fraction of oxidants consumed through methanotrophy. Combining Eqs. S7 and S5 of the SI with Eq. 11, we obtain:

$$\text{COS} = -4 \left(\frac{R_{\text{net}}^{\text{CH}_4} - R_{\text{net}}^{\text{DIC}} - R_{\text{net}}^{\text{Ox}} + R_2}{R_{\text{net}}^{\text{DIC}} + R_{\text{net}}^{\text{CH}_4} + (1 - \chi_M) R_{\text{net}}^{\text{Ox}} - R_2} \right) \quad (12)$$

Introducing the values of $R_{\text{net}}^{\text{CH}_4}$, $R_{\text{net}}^{\text{DIC}}$, $R_{\text{net}}^{\text{Ox}}$ and R_2 (Table 2 and 3) into Eq. 12, we calculate COS values of -3.2 and -0.9 for the Z₁ and Z₂ of Lake Tantaré Basin A, respectively, and of -1.0 to -1.1 for the Z₁ of Lake Bédard, respectively. Note that we were unable to constrain with Eq. 12 the COS for the Z₂ of Lake Bédard since we had to assume a COS value to estimate R_2 and the COS has no influence of the modelled $\delta^{13}\text{C}$ profiles (section S2.2.2.3 of the SI). Negative COS values between -0.9 and -1.1 suggest that fermenting OM in the sediments of the two lake basins would be better represented by a mixture of fatty acids and fatty alcohols than by carbohydrates, as suggested by Clayer et al. (2018) for the sporadically anoxic Lake Tantaré Basin B. For its part, the highly negative COS value of -3.2 calculated for the Z₁ of Lake Tantaré Basin A is unreasonable, and the inaccuracy of the COS determination in this lake basin is discussed in section 4.3.

375 4.3 Reduced organic compounds as methanogenic substrates in lake sediments

In order to better appraise the COS of the fermenting OM in lakes, relevant datasets of porewater solute concentration profiles were gathered from our data repository and from a thorough literature search. To be able to obtain by reactive-transport modeling the $R_{\text{net}}^{\text{solute}}$ required to calculate the COS with Eq. 12, the datasets had to: (i) comprise porewater concentration profiles of CH₄ and DIC and, ideally, those of the EAs; (ii) reveal a net methanogenesis zone, and (iii) enable the carbonate precipitation/dissolution contribution to the DIC concentrations to be estimated. Detailed information on the origin and processing of the 17 selected datasets, acquired in 6 different lake basins from one sub-alpine and three boreal lakes sampled at various dates and/or depths, is given in section S3 of the SI. The CH₄ and DIC porewater profiles determined at hypolimnetic sites of these lake basins and their modeling with the code PROFILE are shown in Fig. 4, whereas the $R_{\text{net}}^{\text{CH}_4}$, $R_{\text{net}}^{\text{DIC}}$ and $R_{\text{net}}^{\text{Ox}}$ values determined from this modeling are regrouped in Table 4. The COS values displayed in Table 4 for all lake basins and dates were calculated by substituting the appropriate $R_{\text{net}}^{\text{CH}_4}$, $R_{\text{net}}^{\text{DIC}}$ and $R_{\text{net}}^{\text{Ox}}$ values in Eq. 12 and assuming that $R_2 = 0$. This latter



assumption was not required Lake Tantaré Basin A (October 2015) and Lake Bédard (October 2015) for which R_2 values were known (Table 4). Equation 12 indicates that any DIC contribution from r_2 would yield lower COS values than those reported in Table 4. The value of χ_M was assumed to be alternately 0 and 1 to provide a range of COS values. The only exception was Lake Tantaré Basin A in October 2015 for which χ_M is known to be 0.75 (section S2.2.2.2 of the SI). Note that although Eq. 12 was derived with the assumption that methanogenesis was hydrogenotrophic ($\chi_H = 1$), assuming that CH_4 was produced by acetoclasty ($\chi_H = 0$) would yield the same expression.

According to Table 4 the COS values are systematically negative at all dates for Lake Tantaré Basin B, Lake Bédard, Jacks Lake and the two sites of Lake Lugano, and they vary generally between -0.9 and -1.9 , with the exception of a value of -2.5 obtained for Lake Tantaré Basin B in July 2007. This latter value is likely too low to be representative of fermenting material and should be rejected. The mean (\pm SD) COS values are -1.7 ± 0.4 for Lake Tantaré Basin B, -1.4 ± 0.4 for Lake Bédard, -1.4 ± 0.2 for Jacks Lake and -1.4 ± 0.3 for Lake Lugano. These COS values, representative of a mixture of fatty acids (COS of -1.0 for C4-fatty acids to about -1.87 for C32-fatty acids) and of fatty alcohols (COS = -2.00), strongly supports the idea that methanogenesis in boreal lakes sediments, as well as in the sediments of other types of lakes, is fueled by more reduced organic compounds than glucose. Lipids such as fatty acids and fatty alcohols with similar COS are naturally abundant in sediments to sustain the estimated rates of CH_4 and DIC production during fermentation (Hedges and Oades, 1997; Cranwell, 1981; Matsumoto, 1989; Burdige, 2006). As discussed by Clayer et al. (2018) the most labile organic compounds (i.e., proteins and carbohydrates) can be rapidly degraded during their transport through the water column and in the uppermost sediment layer, leaving mainly lipids as metabolizable substrates at depths where fermentation and methanogenesis occurs. This interpretation is consistent with thermodynamic and kinetic evidences that proteins and carbohydrates are more labile and are degraded faster than lipids (LaRowe and Van Cappellen, 2011).

The COS values determined for the perennially oxygenated Basin A of Lake Tantaré (mean of -0.6 ± 1.1 ; range of -3.2 to 2.1 ; Table 4) are much more variable than for the five other lake basins which undergo seasonal anoxia. Moreover, the COS values estimated for October 2015 in the Z_1 (-3.2), September 2016 (0.4 – 0.6) and October 2005 (1.8 – 2.1) are unrealistic. Indeed, the very negative value of -3.2 does not correspond to any degradable compound under anoxic conditions, whereas the positive values of 0.4 – 0.6 and 1.8 – 2.1 would involve either amino acids and nucleotides which are very labile (Larowe and Van Cappellen 2011) and tend to be degraded in the water column (Burdige 2007) or oxidized compounds, such as ketones, aldehydes and esters, known to be quickly reduced to alcohols. These observations indicate that the COS determination in this lake basin is unreliable. The misestimation of the COS can probably not be explained by the presence of O_2 itself at the sediment surface of Lake Tantaré Basin A. Indeed, the sediment surface was also oxic at the sites Melide and Figino of Lake Lugano in March 1989 (Table 4) as revealed by detectable bottom water $[\text{O}_2]$ (Table 4), and by low $[\text{Fe}]$, undetectable $\Sigma\text{S}(-\text{II})$ and $[\text{CH}_4]$ and relatively high $[\text{SO}_4^{2-}]$ in overlying water (Lazzaretti et al., 1992; Lazzaretti-Ulmer and Hanselmann, 1999). Despite this, the COS values determined for the two sites of Lake Lugano appear to be realistic and coherent with those calculated for Lakes Tantaré Basin B, Bédard and Jacks. However, we know that benthic organisms are present in Lake Tantaré Basin A (Hare et al., 1994) but lacking at the two sites of Lake Lugano, as shown by the presence of varves (Span et al., 1992)



420 and the absence of benthos remains in the recent sediments at these sites (Niessen et al., 1992). Clayer et al. (2016) provided
evidences that sediment irrigation by benthic animals is effective in Lake Tantaré Basin A and that it should be taken into
account in modeling the porewater solutes profiles. However, these authors also point out the difficulty to properly estimate
the magnitude of solute transport by bioirrigation. The term used in Eq. 2 to calculate this contribution, i.e., $\phi\alpha_{\text{irrigation}}$
425 $([\text{solute}]_{\text{tube}} - [\text{solute}])$, is indeed an approximation of intricate 3-D processes (Meile et al. 2005). And, in the conceptualization
of this bioirrigation term, it was notably assumed that benthic animals continuously irrigate their tubes to maintain solute
concentrations in their biogenic structures ($[\text{solute}]_{\text{tube}}$) identical to those in the water overlying the sediments. But
microbenthic animals are generally reported to irrigate the sediments in a discontinuous manner and the solute concentrations
in their biogenic structures may be highly variable with time (Boudreau and Marinelli 1994; Forster and Graf 1995; Riisgård
and Larsen 2005; Gallon et al. 2008). Hence, owing to the imperfection of the representation of bioirrigation in Eq. 2, COS
430 values estimated for the sediment of Lake Tantaré Basin A should be treated with caution, especially in the Z_1 where the
bioirrigation coefficient takes the highest value. Another potential bias in the estimation of COS values for the oxygenated
basin is the possibility of DIC production through HMW OM fermentation (reaction r2; Corbett et al. 2013). Note that fitting
with Eq. 6 the experimental $\delta^{13}\text{C}$ data does not allow partitioning the production of DIC between r1 and r2 since the two
processes share the same value of fractionation factor ($\alpha_1 = \alpha_2 = 1.000$). It was possible to attribute unequivocally the excess
435 of DIC production rate over that of CH_4 production in the Z_2 of Lake Bédard in October 2015 (Table 4 and Section S2.1.2.2
of the SI) to HMW OM fermentation merely because $R_{\text{net}}^{\text{Ox}}$ was negligible compared to $R_{\text{net}}^{\text{CH}_4}$ and $R_{\text{net}}^{\text{DIC}}$, which is not the case
for Lake Tantaré Basin A (Table 4). Equation 12 indicates that to obtain negative COS values for Lake Tantaré Basin A in
September 2006 and October 2005, R_2 should be $>11 \text{ fmol cm}^{-2} \text{ s}^{-1}$ and $>110 \text{ fmol cm}^{-2} \text{ s}^{-1}$, respectively. These R_2 values
correspond to transferring $>9\%$ and $>44\%$ of the rate of DIC production from R_1 to R_2 for September 2006 and October 2005,
440 respectively. The above discussion underlines several factors that can explain the unreliability in the actual COS estimation
for the perennially oxic Lake Tantaré Basin A, and further research is needed to better assess the importance of these factors.
However, it does not dismiss that the substrate for methanogenesis in this lake basin may have a negative COS value.

5 Conclusions

Our results show that fermentation and methanogenesis represent nearly 50% and 100% of OM mineralization in the top 25
445 cm of the sediments at the hypolimnetic sites in Lake Bédard and in Basin A of Lake Tantaré, respectively and that methane
is produced only by hydrogenotrophy at these two sites. An earlier study reached similar conclusions about the pathways of
methanogenesis and the contribution of this process in OM mineralization in Basin B of Lake Tantaré (Clayer et al. 2018).
Reactive-transport modelling of porewater solutes from three boreal lakes, i.e., Bédard, Tantaré (Basin B) and Jacks, as well
as of the sub-alpine Lake Lugano (Melide and Figino sites) consistently showed that the main substrates for sediment
450 methanogenesis at deep seasonally anoxic hypolimnetic sites have a mean COS value of -1.4 ± 0.3 . Mineralization of the most



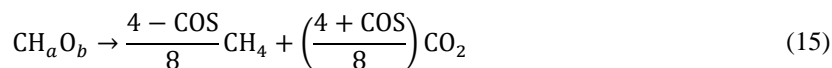
labile compounds during OM downward migration in the water column and in the uppermost sediment layers likely explains why reduced organic compounds fuel methanogenesis in these sediments.

The current representation of the fermenting OM, i.e., CH_2O , in process-based biogeochemical models entails a significant risk of misestimating sedimentary CH_4 and CO_2 production and release to the bottom water and, to a certain extent, of
455 mispredicting evasion of these greenhouse gases to the atmosphere under transient environmental scenarios. To better constrain CH_4 and CO_2 production within sediments, we suggest taking specifically into account the COS of the fermenting OM in formulating the reactions of methanogenesis associated with fermentation in these models. For example, the rates of CH_4 (R^{CH_4}) and DIC (R^{DIC}) production during fermentation coupled to hydrogenotrophy can be expressed as:

$$R^{\text{CH}_4} = R_4 = \frac{4 - \text{COS}}{8} R_1 \quad (13)$$

$$R^{\text{DIC}} = R_1 - R_4 = R_1 \left(1 - \frac{4 - \text{COS}}{8} \right) \quad (14)$$

Given these rate expressions, the stoichiometric formulation of a typical fermentation reaction producing methane becomes:



460 where $a = 2 - \frac{\text{COS}}{2}$, $b = 1 + \frac{\text{COS}}{4}$. Note that the same stoichiometric formulation would be obtained for acetoclastic methanogenesis.

The approach used to estimate the COS of the fermenting OM, although successful for the seasonally anoxic basins, failed to produce reliable COS values when applied to the perennially oxygenated Basin A of Lake Tantaré. We attribute this peculiarity to a misestimation and/or misrepresentation of the benthic irrigation and to the impossibility to partition the DIC production
465 between reactions r1 and r2 which share the same fractionation factor value. Similar problems would likely be encountered also in other lake ecosystems such as epilimnetic sediments and wetlands where solute transport processes remain ill-known. Indeed, these shallow aquatic environments are subject to enhanced benthic activity (Hare 1995), to plant-mediated transport of CH_4 and O_2 (Chanton et al. 1989; Wang et al. 2006), as well as to turbulence (Poindexter et al. 2016) which complicates the estimation of CH_4 and CO_2 production and consumption rates. Hence, the remaining challenge resides in the robust estimations
470 the COS of the fermenting OM in epilimnetic sediments and shallow freshwater environments (e.g., ponds, wetlands), since these environments were shown to be the main contributors to freshwater CH_4 release to the atmosphere (Del Sontro et al., 2016, Bastviken et al., 2008). One potential solution is to investigate trends in the oxygen isotope signatures in the sedimentary DIC in addition to $\delta^{13}\text{C}$ values since it is also influenced by the source of the OM undergoing degradation (e.g., Sauer et al., 2001).



475 **Data availability:**

Upon acceptance, readers will be able to access the data at this url:
<https://www.hydroshare.org/resource/38e069761d7b4cf4abe3cbcaaac06016/>. A proper reference with a DOI will be made available to cite this dataset if the present paper is accepted.

Author contribution:

480 Conceptualization: FC, AT, and CG. Data curation: FC and AT. Formal analysis: FC and AT. Funding acquisition: CG, YG and AT. Investigation: FC and YG. Methodology: AT, CG, YG and FC. Project administration: CG. Resources: CG and YG. Software: FC. Supervision: CG, AT and YG. Validation: AT. Writing – original draft: FC and AT. Writing – review & editing: All.

Competing interests:

485 The authors declare that they have no conflict of interest.

Acknowledgments

We thank P. Boissinot, L. Rancourt, P. Girard, J.-F. Dutil, S. Duval, A. Royer-Lavallée, A. Laberge and A. Barber for research and field work assistance. We are also thankful to J.-F. Hélie, from the Laboratoire de géochimie des isotopes stables légers (UQÀM), who graciously calibrated our $\delta^{13}\text{C}$ internal standard. This work was supported by grants to C.G., A.T. and Y.G.
490 from the Natural Sciences and Engineering Research Council of Canada and the Fonds de Recherche Québécois – Nature et Technologies. Permission from the Québec Ministère du Développement durable, de l'Environnement et de la Lutte contre les changements climatiques to work in the Tantaré Ecological Reserve is gratefully acknowledged.

References

Alperin, M. J., Albert, D. B., & Martens, C. S. (1994). Seasonal variations in production and consumption rates of dissolved
495 organic carbon in an organic-rich coastal sediment. *Geochimica et Cosmochimica Acta*, 58(22), 4909–4930.
[https://doi.org/10.1016/0016-7037\(94\)90221-6](https://doi.org/10.1016/0016-7037(94)90221-6)
Alperin, M. J., Reeburgh, W. S., & Whiticar, M. J. (1988). Carbon and hydrogen isotope fractionation resulting from anaerobic methane oxidation. *Global Biogeochemical Cycles*, 2(3), 279–288. <https://doi.org/10.1029/GB002i003p00279>



- Arndt, S., Jørgensen, B. B., LaRowe, D. E., Middelburg, J. J., Pancost, R. D., & Regnier, P. (2013). Quantifying the degradation
500 of organic matter in marine sediments: A review and synthesis. *Earth-Science Reviews*, 123, 53–86.
<https://doi.org/10.1016/j.earscirev.2013.02.008>
- Arning, E. T., van Berk, W., & Schulz, H.-M. (2016). Fate and behaviour of marine organic matter during burial of anoxic
sediments: Testing CH₂O as generalized input parameter in reaction transport models. *Marine Chemistry*, 178, 8–21.
<https://doi.org/10.1016/j.marchem.2015.12.002>
- 505 Barbieri, A., & Mosello, R. (1992). Chemistry and trophic evolution of Lake Lugano in relation to nutrient budget. *Aquatic
Sciences*, 54(3), 219–237. <https://doi.org/10.1007/BF00878138>
- Bastviken, D., Cole, J. J., Pace, M. L., & Van de Bogert, M. C. (2008). Fates of methane from different lake habitats:
Connecting whole-lake budgets and CH₄ emissions. *Journal of Geophysical Research: Biogeosciences*, 113(G2).
<https://doi.org/10.1029/2007JG000608>
- 510 Bastviken, D., Cole, J., Pace, M., & Tranvik, L. (2004). Methane emissions from lakes: Dependence of lake characteristics,
two regional assessments, and a global estimate. *Global Biogeochemical Cycles*, 18(4).
<https://doi.org/10.1029/2004GB002238>
- Beal, E. J., House, C. H., & Orphan, V. J. (2009). Manganese- and iron-dependent marine methane oxidation. *Science (New
York, N.Y.)*, 325(5937), 184–187. <https://doi.org/10.1126/science.1169984>
- 515 Berg, P., Risgaard-Petersen, N., & Rysgaard, S. (1998). Interpretation of measured concentration profiles in sediment pore
water. *Limnology and Oceanography*, 43(7), 1500–1510. <https://doi.org/10.4319/lo.1998.43.7.1500>
- Blair, N. E., & Carter, W. D. (1992). The carbon isotope biogeochemistry of acetate from a methanogenic marine sediment.
Geochimica et Cosmochimica Acta, 56(3), 1247–1258. [https://doi.org/10.1016/0016-7037\(92\)90060-V](https://doi.org/10.1016/0016-7037(92)90060-V)
- Borowski, W. S., Paull, C. K., & Ussler, W. (1997). Carbon cycling within the upper methanogenic zone of continental rise
520 sediments; An example from the methane-rich sediments overlying the Blake Ridge gas hydrate deposits. *Marine Chemistry*,
57(3), 299–311. [https://doi.org/10.1016/S0304-4203\(97\)00019-4](https://doi.org/10.1016/S0304-4203(97)00019-4)
- Bottinga, Y. (1969). Calculated fractionation factors for carbon and hydrogen isotope exchange in the system calcite-carbon
dioxide-graphite-methane-hydrogen-water vapor. *Geochimica et Cosmochimica Acta*, 33(1), 49–64.
[https://doi.org/10.1016/0016-7037\(69\)90092-1](https://doi.org/10.1016/0016-7037(69)90092-1)
- 525 Boudreau, B., & Marinelli, R. (1994). A modeling study of discontinuous biological irrigation. *Journal of Marine Research*,
52, 947–968. <https://doi.org/10.1357/0022240943076902>
- Boudreau, B. P. (1997). *Diagenetic models and their implementation: modelling transport and reactions in aquatic sediments*.
Springer.
- Burdige, D. J. (2007). Preservation of Organic Matter in Marine Sediments: Controls, Mechanisms, and an Imbalance in
530 Sediment Organic Carbon Budgets? *Chemical Reviews*, 107(2), 467–485. <https://doi.org/10.1021/cr050347q>
- Burdige, D. J., & Komada, T. (2011). Anaerobic oxidation of methane and the stoichiometry of remineralization processes in
continental margin sediments. *Limnology and Oceanography*, 56(5), 1781–1796. <https://doi.org/10.4319/lo.2011.56.5.1781>



- Burdige, D., Komada, T., Magen, C., & Chanton, J. P. (2017). Methane dynamics in Santa Barbara Basin (USA) sediments as examined with a reaction-transport model. *Journal of Marine Research*, *74*, 277–313.
- 535 Carignan, R., & Lean, D. R. S. (1991). Regeneration of dissolved substances in a seasonally anoxic lake: The relative importance of processes occurring in the water column and in the sediments. *Limnology and Oceanography*, *36*(4), 683–707. <https://doi.org/10.4319/lo.1991.36.4.0683>
- Carignan, R., Rapin, F., & Tessier, A. (1985). Sediment porewater sampling for metal analysis: A comparison of techniques. *Geochimica et Cosmochimica Acta*, *49*(11), 2493–2497. [https://doi.org/10.1016/0016-7037\(85\)90248-0](https://doi.org/10.1016/0016-7037(85)90248-0)
- 540 Carmichael, M. J., Bernhardt, E. S., Bräuer, S. L., & Smith, W. K. (2014). The role of vegetation in methane flux to the atmosphere: should vegetation be included as a distinct category in the global methane budget? *Biogeochemistry*, *119*(1), 1–24. <https://doi.org/10.1007/s10533-014-9974-1>
- Chanton, J. P., Whiting, G. J., Blair, N. E., Lindau, C. W., & Bollich, P. K. (1997). Methane emission from rice: Stable isotopes, diurnal variations, and CO₂ exchange. *Global Biogeochemical Cycles*, *11*(1), 15–27. <https://doi.org/10.1029/96GB03761>
- 545 Chanton, J. P., Martens, C. S., & Kelley, C. A. (1989). Gas transport from methane-saturated, tidal freshwater and wetland sediments. *Limnology and Oceanography*, *34*(5), 807–819. <https://doi.org/10.4319/lo.1989.34.5.0807>
- Chasar, L. S., Chanton, J. P., Glaser, P. H., Siegel, D. I., & Rivers, J. S. (2000). Radiocarbon and stable carbon isotopic evidence for transport and transformation of dissolved organic carbon, dissolved inorganic carbon, and CH₄ in a northern Minnesota peatland. *Global Biogeochemical Cycles*, *14*(4), 1095–1108. <https://doi.org/10.1029/1999GB001221>
- 550 Clayer, F., Moritz, A., Gelinas, Y., Tessier, A., & Gobeil, C. (2018). Modeling the carbon isotope signatures of methane and dissolved inorganic carbon to unravel mineralization pathways in boreal lake sediments. *Geochimica Et Cosmochimica Acta*, *229*, 36–52. <https://doi.org/10.1016/j.gca.2018.02.012>
- Clayer, F., Gobeil, C., & Tessier, A. (2016). Rates and pathways of sedimentary organic matter mineralization in two basins of a boreal lake: Emphasis on methanogenesis and methanotrophy: Methane cycling in boreal lake sediments. *Limnology and*
- 555 *Oceanography*, *61*(S1), S131–S149. <https://doi.org/10.1002/lno.10323>
- Cole, J. J., Prairie, Y. T., Caraco, N. F., McDowell, W. H., Tranvik, L. J., Striegl, R. G., et al. (2007). Plumbing the Global Carbon Cycle: Integrating Inland Waters into the Terrestrial Carbon Budget. *Ecosystems*, *10*(1), 172–185. <https://doi.org/10.1007/s10021-006-9013-8>
- Conrad, R. (1999). Contribution of hydrogen to methane production and control of hydrogen concentrations in methanogenic soils and sediments. *FEMS Microbiology Ecology*, *28*(3), 193–202. <https://doi.org/10.1111/j.1574-6941.1999.tb00575.x>
- 560 Conrad, R., Claus, P., Chidthaisong, A., Lu, Y., Fernandez Scavino, A., Liu, Y., et al. (2014). Stable carbon isotope biogeochemistry of propionate and acetate in methanogenic soils and lake sediments. *Organic Geochemistry*, *73*, 1–7. <https://doi.org/10.1016/j.orggeochem.2014.03.010>
- Conrad, R. (2005). Quantification of methanogenic pathways using stable carbon isotopic signatures: a review and a proposal. *Organic Geochemistry*, *36*(5), 739–752. <https://doi.org/10.1016/j.orggeochem.2004.09.006>
- 565



- Conrad, R., Chan, O.-C., Claus, P., & Casper, P. (2007). Characterization of methanogenic Archaea and stable isotope fractionation during methane production in the profundal sediment of an oligotrophic lake (Lake Stechlin, Germany). *Limnology and Oceanography*, 52(4), 1393–1406. <https://doi.org/10.4319/lo.2007.52.4.1393>
- 570 Conrad, R., Claus, P., & Casper, P. (2009). Characterization of stable isotope fractionation during methane production in the sediment of a eutrophic lake, Lake Dagow, Germany. *Limnology and Oceanography*, 54(2), 457–471. <https://doi.org/10.4319/lo.2009.54.2.0457>
- Conrad, R., Klose, M., Yuan, Q., Lu, Y., & Chidthaisong, A. (2012). Stable carbon isotope fractionation, carbon flux partitioning and priming effects in anoxic soils during methanogenic degradation of straw and soil organic matter. *Soil Biology and Biochemistry*, 49, 193–199. <https://doi.org/10.1016/j.soilbio.2012.02.030>
- 575 Corbett, J. E., Tfaily, M. M., Burdige, D. J., Cooper, W. T., Glaser, P. H., & Chanton, J. P. (2013). Partitioning pathways of CO₂ production in peatlands with stable carbon isotopes. *Biogeochemistry*, 114, 327–340. Retrieved from JSTOR.
- Corbett, J. E., Tfaily, M. M., Burdige, D. J., Glaser, P. H., & Chanton, J. P. (2015). The relative importance of methanogenesis in the decomposition of organic matter in northern peatlands. *Journal of Geophysical Research: Biogeosciences*, 120(2), 280–293. <https://doi.org/10.1002/2014JG002797>
- 580 Couture, R.-M., Fischer, R., Van Cappellen, P., & Gobeil, C. (2016). Non-steady state diagenesis of organic and inorganic sulfur in lake sediments. *Geochimica et Cosmochimica Acta*, 194, 15–33. <https://doi.org/10.1016/j.gca.2016.08.029>
- Couture, R.-M., Gobeil, C., & Tessier, A. (2008). Chronology of Atmospheric Deposition of Arsenic Inferred from Reconstructed Sedimentary Records. *Environmental Science & Technology*, 42(17), 6508–6513. <https://doi.org/10.1021/es800818j>
- 585 Cranwell, P. A. (1981). Diagenesis of free and bound lipids in terrestrial detritus deposited in a lacustrine sediment. *Organic Geochemistry*, 3(3), 79–89. [https://doi.org/10.1016/0146-6380\(81\)90002-4](https://doi.org/10.1016/0146-6380(81)90002-4)
- D’arcy, P. (1993). *Relations entre les propriétés du bassin versant, la morphométrie du lac et la qualité des eaux*. INRS-ETE, Université du Québec, Québec City, Québec, Canada.
- DelSontro, T., Boutet, L., St-Pierre, A., del Giorgio, P. A., & Prairie, Y. T. (2016). Methane ebullition and diffusion from northern ponds and lakes regulated by the interaction between temperature and system productivity: Productivity regulates methane lake flux. *Limnology and Oceanography*, 61(S1), S62–S77. <https://doi.org/10.1002/lno.10335>
- 590 Duan, Z., & Mao, S. (2006). A thermodynamic model for calculating methane solubility, density and gas phase composition of methane-bearing aqueous fluids from 273 to 523K and from 1 to 2000bar. *Geochimica et Cosmochimica Acta*, 70(13), 3369–3386. <https://doi.org/10.1016/j.gca.2006.03.018>
- 595 Egger, M., Rasigraf, O., Sapart, C. J., Jilbert, T., Jetten, M. S. M., Röckmann, T., et al. (2015). Iron-Mediated Anaerobic Oxidation of Methane in Brackish Coastal Sediments. *Environmental Science & Technology*, 49(1), 277–283. <https://doi.org/10.1021/es503663z>
- Emrich, K., Ehhalt, D. H., & Vogel, J. C. (1970). Carbon isotope fractionation during the precipitation of calcium carbonate. *Earth and Planetary Science Letters*, 8(5), 363–371. [https://doi.org/10.1016/0012-821X\(70\)90109-3](https://doi.org/10.1016/0012-821X(70)90109-3)



- 600 Ettwig, K. F., Butler, M. K., Le Paslier, D., Pelletier, E., Mangenot, S., Kuypers, M. M. M., et al. (2010). Nitrite-driven anaerobic methane oxidation by oxygenic bacteria. *Nature*, 464(7288), 543–548. <https://doi.org/10.1038/nature08883>
- Feyte, S., Gobeil, C., Tessier, A., & Cossa, D. (2012). Mercury dynamics in lake sediments. *Geochimica et Cosmochimica Acta*, 82, 92–112. <https://doi.org/10.1016/j.gca.2011.02.007>
- Forster, S., & Graf, G. (1995). Impact of irrigation on oxygen flux into the sediment: intermittent pumping by Callianassa subterranea and “piston-pumping” by Lanice conchilega. *Marine Biology*, 123(2), 335–346. <https://doi.org/10.1007/BF00353625>
- 605 Galand, P. E., Yrjälä, K., & Conrad, R. (2010). Stable carbon isotope fractionation during methanogenesis in three boreal peatland ecosystems. *Biogeosciences*, 7(11), 3893–3900. <https://doi.org/10.5194/bg-7-3893-2010>
- Gallon, C., Hare, L., & Tessier, A. (2008). Surviving in anoxic surroundings: how burrowing aquatic insects create anoxic microhabitat. *Journal of the North American Benthological Society*, 27(3), 570–580. <https://doi.org/10.1899/07-132.1>
- 610 Gelwicks, J. T., Risatti, J. B., & Hayes, J. M. (1994). Carbon isotope effects associated with acetoclastic methanogenesis. *Applied and Environmental Microbiology*, 60(2), 467–472.
- Ghosh, P., & Brand, W. A. (2003). Stable isotope ratio mass spectrometry in global climate change research. *International Journal of Mass Spectrometry*, 228(1), 1–33. [https://doi.org/10.1016/S1387-3806\(03\)00289-6](https://doi.org/10.1016/S1387-3806(03)00289-6)
- 615 Gobeil, C., Tessier, A., & Couture, R.-M. (2013). Upper Mississippi Pb as a mid-1800s chronostratigraphic marker in sediments from seasonally anoxic lakes in Eastern Canada. *Geochimica et Cosmochimica Acta*, 113, 125–135. <https://doi.org/10.1016/j.gca.2013.02.023>
- Happell, J. D., Chanton, J. P., & Showers, W. J. (1995). Methane transfer across the water-air interface in stagnant wooded swamps of Florida: Evaluation of mass-transfer coefficients and isotopic fractionation. *Limnology and Oceanography*, 40(2), 290–298. <https://doi.org/10.4319/lo.1995.40.2.0290>
- 620 Hare, L. (1995). Sediment Colonization by Littoral and Profundal Insects. *Journal of the North American Benthological Society*, 14, 315. <https://doi.org/10.2307/1467783>
- Hare, L., Carignan, R., & Huerta-Diaz, M. A. (1994). A field study of metal toxicity and accumulation by benthic invertebrates; implications for the acid-volatile sulfide (AVS) model. *Limnology and Oceanography*, 39(7), 1653–1668. <https://doi.org/10.4319/lo.1994.39.7.1653>
- 625 Hastie, A., Lauerwald, R., Weyhenmeyer, G., Sobek, S., Verpoorter, C., & Regnier, P. (2018). CO₂ evasion from boreal lakes: Revised estimate, drivers of spatial variability, and future projections. *Global Change Biology*, 24(2), 711–728. <https://doi.org/10.1111/gcb.13902>
- Hedges, J. I., & Oades, J. M. (1997). Comparative organic geochemistries of soils and marine sediments. *Organic Geochemistry*, 27(7), 319–361. [https://doi.org/10.1016/S0146-6380\(97\)00056-9](https://doi.org/10.1016/S0146-6380(97)00056-9)
- 630 Hélie, J.-F. (2004). *Géochimie et flux de carbone organique et inorganique dans les milieux aquatiques de l’est du Canada : exemples du Saint-Laurent et du réservoir Robert-Bourassa : approche isotopique* (Phd, Université du Québec à Chicoutimi). Retrieved from <https://constellation.uqac.ca/672/>



- Hesslein, R. H. (1976). An in situ sampler for close interval pore water studies1. *Limnology and Oceanography*, 21(6), 912–914. <https://doi.org/10.4319/lo.1976.21.6.0912>
- Holgerson, M. A., & Raymond, P. A. (2016). Large contribution to inland water CO₂ and CH₄ emissions from very small ponds. *Nature Geoscience*, 9(3), 222–226. <https://doi.org/10.1038/ngeo2654>
- Holmkvist, L., Ferdelman, T. G., & Jørgensen, B. B. (2011). A cryptic sulfur cycle driven by iron in the methane zone of marine sediment (Aarhus Bay, Denmark). *Geochimica et Cosmochimica Acta*, 75(12), 3581–3599. <https://doi.org/10.1016/j.gca.2011.03.033>
- Hornibrook, E. R. C., Longstaffe, F. J., & Fyfe, W. S. (1997). Spatial distribution of microbial methane production pathways in temperate zone wetland soils: Stable carbon and hydrogen isotope evidence. *Geochimica et Cosmochimica Acta*, 61(4), 745–753. [https://doi.org/10.1016/S0016-7037\(96\)00368-7](https://doi.org/10.1016/S0016-7037(96)00368-7)
- Hornibrook, E. R. C., Longstaffe, F. J., & Fyfe, W. S. (2000). Evolution of stable carbon isotope compositions for methane and carbon dioxide in freshwater wetlands and other anaerobic environments. *Geochimica et Cosmochimica Acta*, 64(6), 1013–1027. [https://doi.org/10.1016/S0016-7037\(99\)00321-X](https://doi.org/10.1016/S0016-7037(99)00321-X)
- Jähne, B., Heinz, G., & Dietrich, W. (1987). Measurement of the diffusion coefficients of sparingly soluble gases in water. *Journal of Geophysical Research: Oceans*, 92(C10), 10767–10776. <https://doi.org/10.1029/JC092iC10p10767>
- Jørgensen, B. B., & Parkes, R. J. (2010). Role of sulfate reduction and methane production by organic carbon degradation in eutrophic fjord sediments (Limfjorden, Denmark). *Limnology and Oceanography*, 55(3), 1338–1352. <https://doi.org/10.4319/lo.2010.55.3.1338>
- Joshani, A. (2015). *Investigating organic matter preservation through complexation with iron oxides in Lake Tantaré* (Masters, Concordia University). Retrieved from <https://spectrum.library.concordia.ca/980434/>
- Kankaala, P., Huotari, J., Tulonen, T., & Ojala, A. (2013). Lake-size dependent physical forcing drives carbon dioxide and methane effluxes from lakes in a boreal landscape. *Limnology and Oceanography*, 58(6), 1915–1930. <https://doi.org/10.4319/lo.2013.58.6.1915>
- Krzycki, J. A., Kenealy, W. R., DeNiro, M. J., & Zeikus, J. G. (1987). Stable Carbon Isotope Fractionation by *Methanosarcina barkeri* during Methanogenesis from Acetate, Methanol, or Carbon Dioxide-Hydrogen. *Applied and Environmental Microbiology*, 53(10), 2597–2599.
- Laforte, L., Tessier, A., Gobeil, C., & Carignan, R. (2005). Thallium diagenesis in lacustrine sediments. *Geochimica et Cosmochimica Acta*, 69(22), 5295–5306. <https://doi.org/10.1016/j.gca.2005.06.006>
- Lapham, L., Proctor, L., & Chanton, J. (1999). Using Respiration Rates and Stable Carbon Isotopes to Monitor the Biodegradation of Orimulsion by Marine Benthic Bacteria. *Environmental Science & Technology*, 33(12), 2035–2039. <https://doi.org/10.1021/es981158a>
- LaRowe, D. E., & Van Cappellen, P. (2011). Degradation of natural organic matter: A thermodynamic analysis. *Geochimica et Cosmochimica Acta*, 75(8), 2030–2042. <https://doi.org/10.1016/j.gca.2011.01.020>



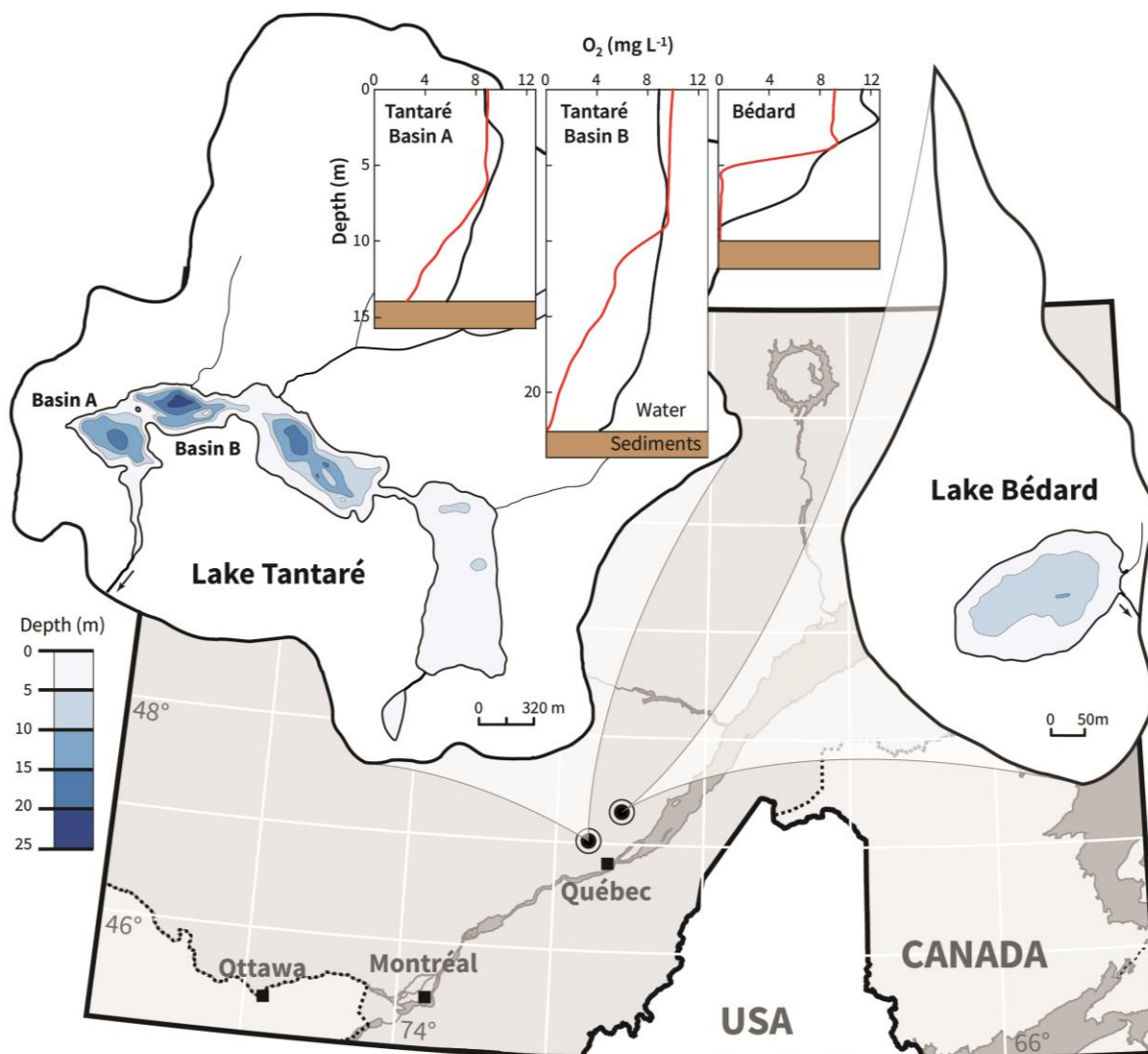
- Lazzaretti, M. A., Hanselmann, K. W., Brandl, H., Span, D., & Bachofen, R. (1992). The role of sediments in the phosphorus cycle in Lake Lugano. II. Seasonal and spatial variability of microbiological processes at the sediment-water interface. *Aquatic Sciences*, 54(3), 285–299. <https://doi.org/10.1007/BF00878142>
- 670 Lazzaretti-Ulmer, M. A., & Hanselmann, K. W. (1999). Seasonal variation of the microbially regulated buffering capacity at sediment-water interfaces in a freshwater lake. *Aquatic Sciences*, 61(1), 59–74. <https://doi.org/10.1007/s000270050052>
- Lettmann, K. A., Riedinger, N., Ramlau, R., Knab, N., Böttcher, M. E., Khalili, A., et al. (2012). Estimation of biogeochemical rates from concentration profiles: A novel inverse method. *Estuarine, Coastal and Shelf Science*, 100, 26–37. <https://doi.org/10.1016/j.ecss.2011.01.012>
- 675 Matsumoto, G. I. (1989). Biogeochemical study of organic substances in Antarctic lakes. *Hydrobiologia*, 172(1), 265–299. <https://doi.org/10.1007/BF00031627>
- Meile, C. D., Berg, P., Cappellen, P. S. J., & Tuncay, K. (2005). Solute-specific pore water irrigation: Implications for chemical cycling in early diagenesis. *Journal of Marine Research*, 63. <https://doi.org/10.1357/0022240054307885>
- Mook, W. G., Bommerson, J. C., & Staverman, W. H. (1974). Carbon isotope fractionation between dissolved bicarbonate and gaseous carbon dioxide. *Earth and Planetary Science Letters*, 22(2), 169–176. [https://doi.org/10.1016/0012-821X\(74\)90078-8](https://doi.org/10.1016/0012-821X(74)90078-8)
- 680 Natchimuthu, S., Wallin, M. B., Klemedtsson, L., & Bastviken, D. (2017). Spatio-temporal patterns of stream methane and carbon dioxide emissions in a hemiboreal catchment in Southwest Sweden. *Scientific Reports*, 7(1). <https://doi.org/10.1038/srep39729>
- 685 Niessen, F., Wick, L., Bonani, G., Chondrogianni, C., & Siegenthaler, C. (1992). Aquatic system response to climatic and human changes: Productivity, bottom water oxygen status, and sapropel formation in Lake Lugano over the last 10 000 years. *Aquatic Sciences*, 54(3), 257–276. <https://doi.org/10.1007/BF00878140>
- Norði, K., Thamdrup, B., & Schubert, C. J. (2013). Anaerobic oxidation of methane in an iron-rich Danish freshwater lake sediment. *Limnology and Oceanography*, 58(2), 546–554. <https://doi.org/10.4319/lo.2013.58.2.0546>
- 690 O’Leary, M. H. (1984). Measurement of the isotope fractionation associated with diffusion of carbon dioxide in aqueous solution. *The Journal of Physical Chemistry*, 88(4), 823–825. <https://doi.org/10.1021/j150648a041>
- Paraska, D. W., Hipsey, M. R., & Salmon, S. U. (2014). Sediment diagenesis models: Review of approaches, challenges and opportunities. *Environmental Modelling & Software*, 61, 297–325. <https://doi.org/10.1016/j.envsoft.2014.05.011>
- Pick, F. R., Lean, D. R. S., & Nalewajko, C. (1984). Nutrient status of metalimnetic phytoplankton peaks. *Limnology and Oceanography*, 29(5), 960–971. <https://doi.org/10.4319/lo.1984.29.5.0960>
- 695 Pohlman, J. W., Ruppel, C., Hutchinson, D. R., Downer, R., & Coffin, R. B. (2008). Assessing sulfate reduction and methane cycling in a high salinity pore water system in the northern Gulf of Mexico. *Marine and Petroleum Geology*, 25(9), 942–951. <https://doi.org/10.1016/j.marpetgeo.2008.01.016>



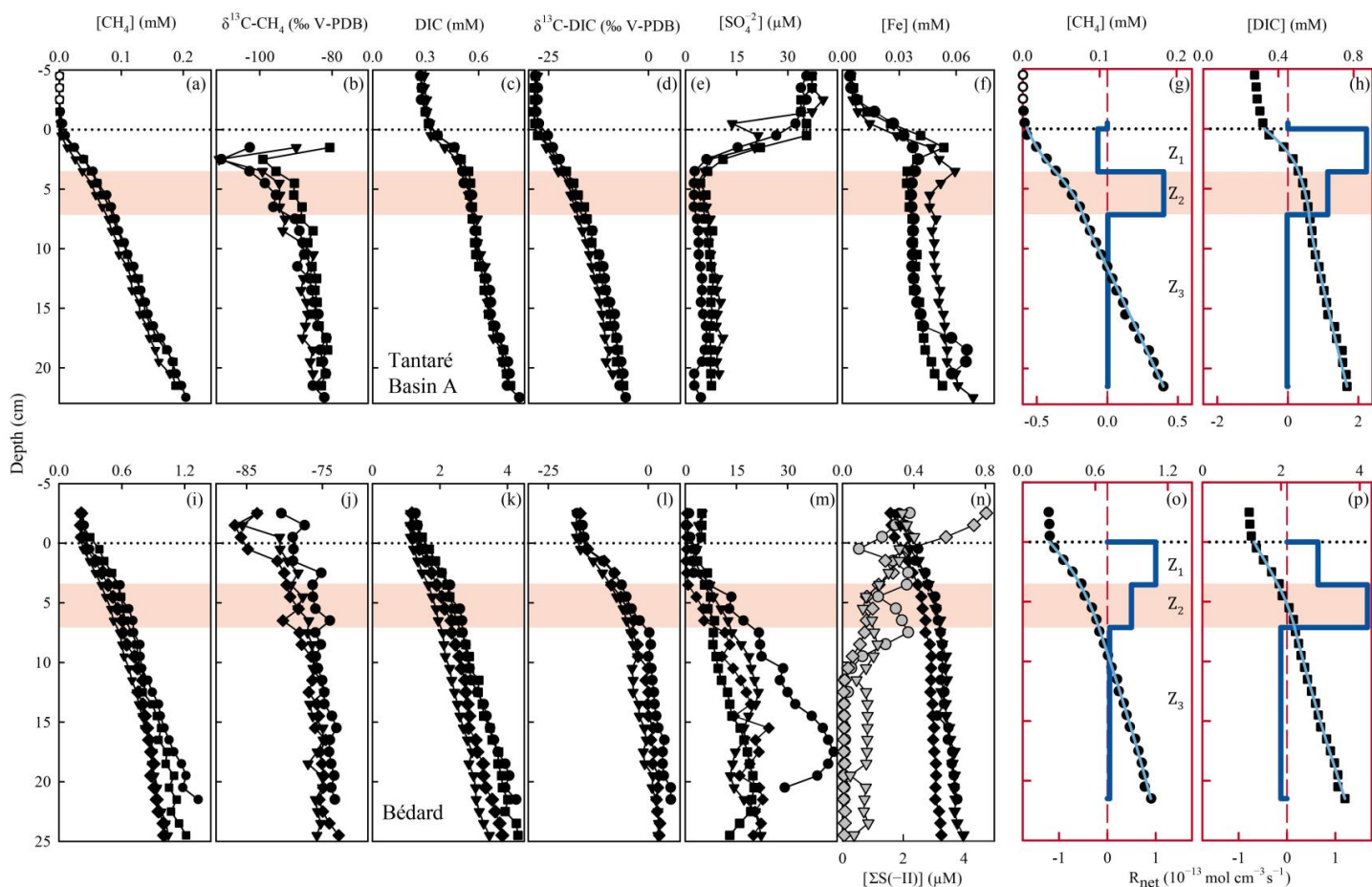
- Pohlman, John W., Riedel, M., Bauer, J. E., Canuel, E. A., Paull, C. K., Lapham, L., et al. (2013). Anaerobic methane oxidation in low-organic content methane seep sediments. *Geochimica et Cosmochimica Acta*, 108, 184–201. <https://doi.org/10.1016/j.gca.2013.01.022>
- Poindexter, C. M., Baldocchi, D. D., Matthes, J. H., Knox, S. H., & Variano, E. A. (2016). The contribution of an overlooked transport process to a wetland's methane emissions. *Geophysical Research Letters*, 43(12), 6276–6284. <https://doi.org/10.1002/2016GL068782>
- Raghoebarsing, A. A., Pol, A., van de Pas-Schoonen, K. T., Smolders, A. J. P., Ettwig, K. F., Rijpstra, W. I. C., et al. (2006). A microbial consortium couples anaerobic methane oxidation to denitrification. *Nature*, 440(7086), 918–921. <https://doi.org/10.1038/nature04617>
- Riisgård, H. U., & Larsen, P. S. (2005). Water pumping and analysis of flow in burrowing zoobenthos: an overview. *Aquatic Ecology*, 39(2), 237–258. <https://doi.org/10.1007/s10452-004-1916-x>
- Sabrekov, A. F., Runkle, B. R. K., Glagolev, M. V., Terentjeva, I. E., Stepanenko, V. M., Kotsyurbenko, O. R., et al. (2017). Variability in methane emissions from West Siberia's shallow boreal lakes on a regional scale and its environmental controls. *Biogeosciences*, 14(15), 3715–3742. <https://doi.org/10.5194/bg-14-3715-2017>
- Sauer, P. E., Miller, G. H., & Overpeck, J. T. (2001). Oxygen isotope ratios of organic matter in arctic lakes as a paleoclimate proxy: field and laboratory investigations. *Journal of Paleolimnology*, 25(1), 43–64. <https://doi.org/10.1023/A:1008133523139>
- Saunois, M., Bousquet, P., Poulter, B., Pregon, A., Ciais, P., Canadell, J. G., et al. (2016). The global methane budget 2000–2012. *Earth System Science Data*, 8(2), 697–751. <https://doi.org/10.5194/essd-8-697-2016>
- Schindler, D. W., Curtis, P. J., Parker, B. R., & Stainton, M. P. (1996). Consequences of climate warming and lake acidification for UV-B penetration in North American boreal lakes. *Nature*, 379(6567), 705–708. <https://doi.org/10.1038/379705a0>
- Sivan, O., Schrag, D. P., & Murray, R. W. (2007). Rates of methanogenesis and methanotrophy in deep-sea sediments. *Geobiology*, 5(2), 141–151. <https://doi.org/10.1111/j.1472-4669.2007.00098.x>
- Span, D., Dominik, J., Lazzaretti, M. A., & Vernet, J.-P. (1992). The role of sediments in the phosphorus cycle in Lake Lugano. I. Geochemical approach. *Aquatic Sciences*, 54(3), 277–284. <https://doi.org/10.1007/BF00878141>
- Staehr, P. A., Testa, J. M., Kemp, W. M., Cole, J. J., Sand-Jensen, K., & Smith, S. V. (2012). The metabolism of aquatic ecosystems: history, applications, and future challenges. *Aquatic Sciences*, 74(1), 15–29. <https://doi.org/10.1007/s00027-011-0199-2>
- Thottathil, S. D., Reis, P. C. J., & Prairie, Y. T. (2019). Methane oxidation kinetics in northern freshwater lakes. *Biogeochemistry*, 143(1), 105–116. <https://doi.org/10.1007/s10533-019-00552-x>
- Tipping, E. (2002). *Cation binding by humic substances*. Cambridge University Press.
- Turner, A. J., Jacob, D. J., Wecht, K. J., Maasackers, J. D., Lundgren, E., Andrews, A. E., et al. (2015). Estimating global and North American methane emissions with high spatial resolution using GOSAT satellite data. *Atmospheric Chemistry and Physics*, 15(12), 7049–7069. <https://doi.org/10.5194/acp-15-7049-2015>



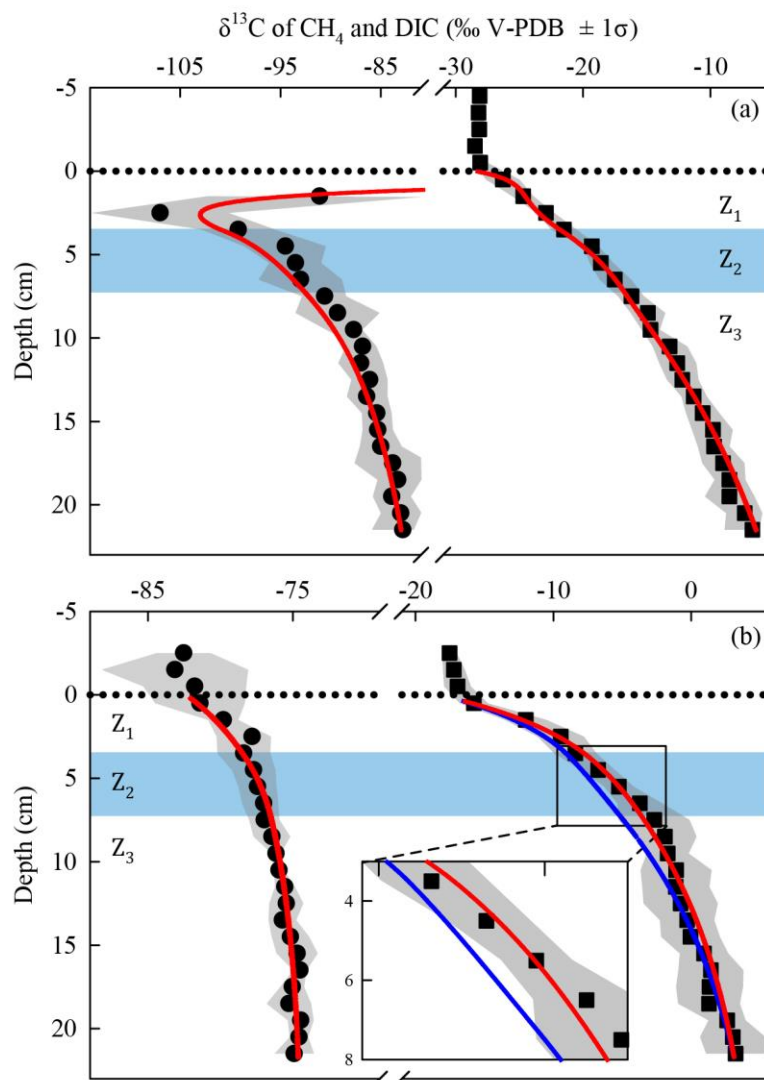
- Ullman, W. J., & Aller, R. C. (1982). Diffusion coefficients in nearshore marine sediments1. *Limnology and Oceanography*, 27(3), 552–556. <https://doi.org/10.4319/lo.1982.27.3.0552>
- 735 Verpoorter, C., Kutser, T., Seekell, D. A., & Tranvik, L. J. (2014). A global inventory of lakes based on high-resolution satellite imagery. *Geophysical Research Letters*, 41(18), 6396–6402. <https://doi.org/10.1002/2014GL060641>
- Wallin, M. B., Campeau, A., Audet, J., Bastviken, D., Bishop, K., Kokic, J., et al. (2018). Carbon dioxide and methane emissions of Swedish low-order streams—a national estimate and lessons learnt from more than a decade of observations. *Limnology and Oceanography Letters*, 3(3), 156–167. <https://doi.org/10.1002/lo2.10061>
- 740 Wand, U., Samarkin, V. A., Nitzsche, H.-M., & Hubberten, H.-W. (2006). Biogeochemistry of methane in the permanently ice-covered Lake Untersee, central Dronning Maud Land, East Antarctica. *Limnology and Oceanography*, 51(2), 1180–1194. <https://doi.org/10.4319/lo.2006.51.2.1180>
- Wang, Y., & Van Cappellen, P. (1996). A multicomponent reactive transport model of early diagenesis: Application to redox cycling in coastal marine sediments. *Geochimica et Cosmochimica Acta*, 60(16), 2993–3014. [https://doi.org/10.1016/0016-7037\(96\)00140-8](https://doi.org/10.1016/0016-7037(96)00140-8)
- 745 Werth, M., & Kuzyakov, Y. (2010). ¹³C fractionation at the root–microorganisms–soil interface: A review and outlook for partitioning studies. *Soil Biology and Biochemistry*, 42(9), 1372–1384. <https://doi.org/10.1016/j.soilbio.2010.04.009>
- Whiticar, M. J., Faber, E., & Schoell, M. (1986). Biogenic methane formation in marine and freshwater environments: CO₂ reduction vs. acetate fermentation—Isotope evidence. *Geochimica et Cosmochimica Acta*, 50(5), 693–709. [https://doi.org/10.1016/0016-7037\(86\)90346-7](https://doi.org/10.1016/0016-7037(86)90346-7)
- 750 Whiticar, M. J. (1999). Carbon and hydrogen isotope systematics of bacterial formation and oxidation of methane. *Chemical Geology*, 161(1), 291–314. [https://doi.org/10.1016/S0009-2541\(99\)00092-3](https://doi.org/10.1016/S0009-2541(99)00092-3)
- Whiticar, M. J., & Faber, E. (1986). Methane oxidation in sediment and water column environments—Isotope evidence. *Organic Geochemistry*, 10(4), 759–768. [https://doi.org/10.1016/S0146-6380\(86\)80013-4](https://doi.org/10.1016/S0146-6380(86)80013-4)
- 755 Wuebbles, D. J., & Hayhoe, K. (2002). Atmospheric methane and global change. *Earth-Science Reviews*, 57(3), 177–210. [https://doi.org/10.1016/S0012-8252\(01\)00062-9](https://doi.org/10.1016/S0012-8252(01)00062-9)
- Deng, A., & Stauffer, D. R. (2006). On improving 4-km mesoscale model simulations. *Journal of Applied Meteorology and Climatology*, 45(3), 361–381. doi:10.1175/JAM2341.1



760 **Figure 1: Location map and bathymetry of Lakes Tantaré and Bédard. The bathymetric map of Lake Tantaré was reproduced from the map C-9287 of the Service des eaux de surface of the Québec Ministry of Environment. The map of Lake Bédard was reproduced from D’Arcy (1993). Dioxygen concentrations in the water column of Lake Tantaré basins A and B, and of Lake Bédard are given for June (black lines) and October (red lines).**



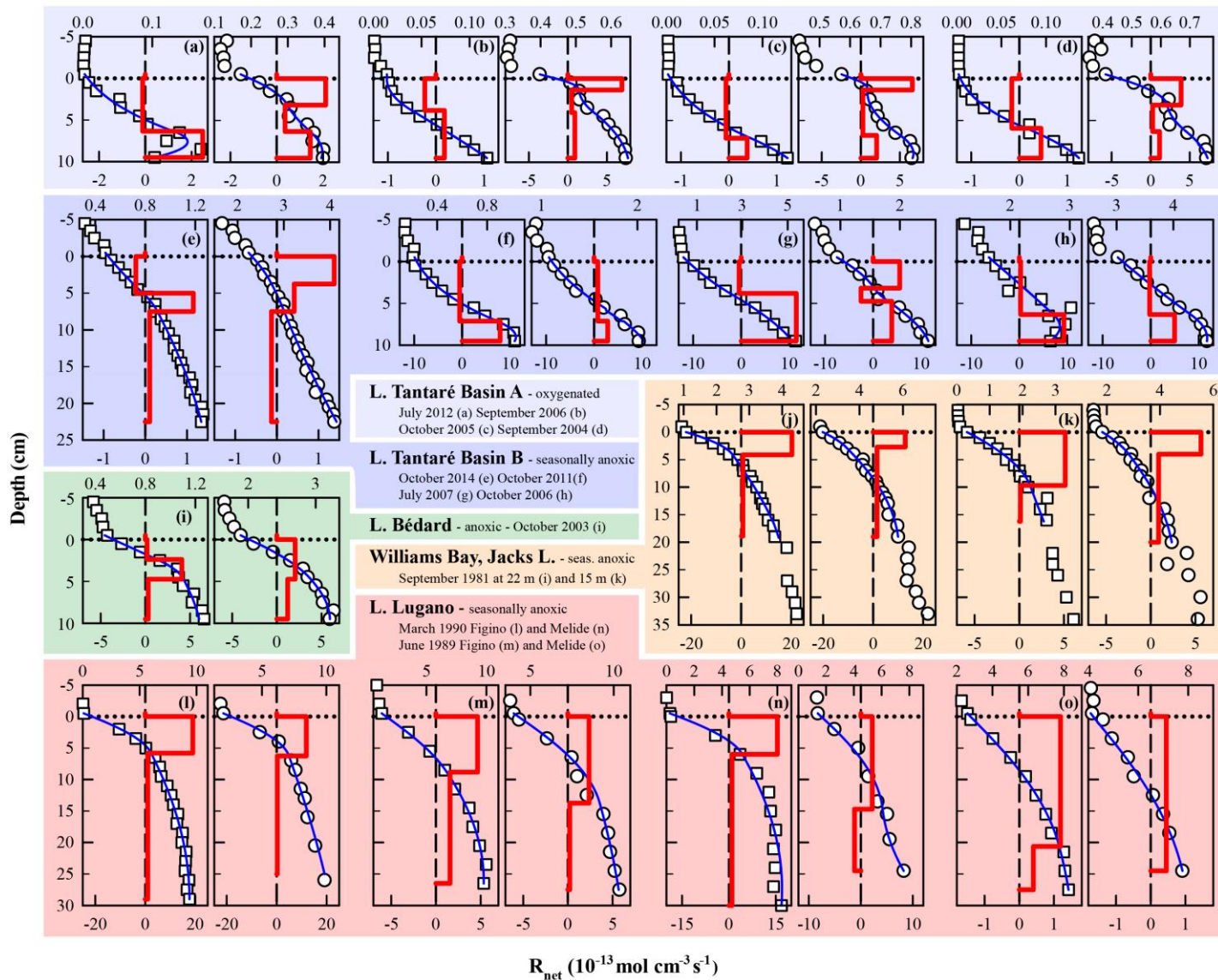
765 **Figure 2 : Replicate porewater profiles of CH_4 (a and i), $\delta^{13}\text{C}-\text{CH}_4$ (b and j), DIC (c and k), $\delta^{13}\text{C}-\text{DIC}$ (d and l), SO_4^{2-} (e and m), Fe and $\Sigma\text{S}(-\text{II})$ (f and n), and comparison of the modeled (blue lines) and average ($n = 3$) measured (symbols) concentration profiles of CH_4 (g and o) and DIC (h and p) in Lakes Tantaré Basin A (a–h) and Bédard (i–p). Different symbols indicate data from different peepers and empty symbols are for concentrations below detection limit. The horizontal dotted line indicates the sediment-water interface. The thick and thin blue lines represent the net solute reaction rate ($R_{\text{net}}^{\text{solute}}$) and the modeled concentration profiles, respectively. The red area fills correspond to the sediment zones Z_2 .**



770 **Figure 3 : Comparison of the simulated (lines) and measured average ($n = 3$) $\delta^{13}\text{C}$ profiles of CH_4 (circles) and DIC (squares) in the porewater of Lake Tantaré Basin A (a) and Lake Bédard (b). The horizontal dotted line indicates the sediment-water interface. The variability in $\delta^{13}\text{C}$ values (\pm one standard deviation – σ) related to the spatial heterogeneity within the sampling area is shown by the grey area fills. The zone Z_2 is delimited by the blue area fill. In panel b, the blue lines are the profiles simulated with the default rate values and optimal α_1 and f values as described in section S2.2.1. The red lines in panel (b) are the profiles simulated with α_2 values of 0.980–0.984 (see section 4.1 for details).**



CH₄ -□- and DIC -○- concentrations (mM)



775 **Figure 4 : Comparison of the modeled (blue lines) and average ($n = 3$) measured concentration profiles of CH₄ (squares) and DIC (circles) in Lakes Tantaré Basin A (a–d) and Basin B (a–h), Bédard (i), Jacks Lake (j–k) and Lake Lugano (l–o) at various sampling dates. The thick red lines represent the net solute reaction rate (R_{net}^{solute}).**



Table 1: Reactions (r1–r8) considered, their reaction rates (R_1 – R_8) and carbon isotopic fractionation factors (α_1 – α_7).

Description	Reaction	ID
CO₂ production due to complete fermentation of labile OM^a		
	$C_xH_yO_z + (x + v_1 - z)H_2O \xrightarrow[\alpha_1]{R_1} \left(\frac{x - v_1}{2}\right)CH_3COOH + v_1CO_2 + \left(\frac{y}{2} - z + 2v_1\right)H_2$	r1
CO₂ production due to partial fermentation of HMW OM^{a,b}		
	$v_2HMW\ OM \xrightarrow[\alpha_2]{R_2} v_3\ LMW\ OM + v_4CO_2$	r2
Methanogenesis via		
acetoclasty	$CH_3COOH \xrightarrow[\alpha_3]{R_3} CH_4 + CO_2$	r3
hydrogenotrophy	$CO_2 + 4H_2 \xrightarrow[\alpha_4]{R_4} CH_4 + 2H_2O$	r4
CO₂ production due to		
methanotrophy	$CH_4 + 2\ Oxidants \xrightarrow[\alpha_5]{R_5} CO_2 + 2\ Reducers$	r5
OM oxidation	$OM + Oxidant \xrightarrow[\alpha_6]{R_6} CO_2 + Reducer$	r6
Precipitation of siderite		
	$Fe^{2+} + CO_2 + H_2O \xrightarrow[\alpha_7]{R_7} FeCO_{3(s)} + 2H^+$	r7
H₂ production through a Fe-S cryptic cycle^{a,c}		
	$(16 + v_5)H_2S + 8FeOOH \xrightarrow{R_8} 8FeS_2 + v_5SO_4^{2-} + (4 + 4v_5)H_2 + (16 - 4v_5)H_2O + 2v_5H^+$	r8

780 ^a where v_1 can have any value between 0 and x , values for v_2 – v_4 are unknown and v_5 can have any value between 0 and 1.

^b HMW OM and LMW OM designate high and lower molecular weight organic matter, respectively.

^c adapted from Holmkvist et al. (2011)



785 **Table 2: Net production rates ($R_{\text{net}}^{\text{solute}}$) of CH₄, DIC and oxidants obtained with the code PROFILE in the three CH₄ consumption/production zones (Z₁, Z₂ and Z₃) for both sampling sites.**

Sampling site	Zones	Depth	$R_{\text{net}}^{\text{DIC}}$	$R_{\text{net}}^{\text{CH}_4}$	$R_{\text{net}}^{\text{Ox}}$
	([O ₂] in mg L ⁻¹)	(cm)	(fmol cm ⁻³ s ⁻¹)		
Tantaré Basin A (2.5)	Z ₁	0–3.6	223	-7	-335
	Z ₂	3.6–7.2	113	39	-103
	Z ₃	7.2–21.5	-2	1	
Bédard (<0.1)	Z ₁	0–3.6	65	100	-6.5
	Z ₂	3.6–7.2	167	50	-4.5
	Z ₃	7.2–21.5	-13	5	



Table 3: Molecular diffusivity ratio of CH₄ (f-CH₄) as well as the isotopic fractionation factors (α_1 , α_2 , α_4 – α_7) and rates (R₁, R₂, R₄–R₇; fmol cm⁻³ s⁻¹) of each reaction involved in OM mineralization in each zone and for the whole sediment column (ΣR_i ; fmol cm⁻² s⁻¹) corresponding to the lowest values of N_{res}. At both study sites, R₃ was shown to be negligible. See section S2 of the SI for details.

Study site	Zones	f-CH ₄	α_1	α_2	α_4	α_5	α_6	α_7	R ₁	R ₂	R ₄	R ₅	R ₆	R ₇
Tantaré	Z ₁	1.003	1.000	-	1.094	1.024	1.000	-	132	-	119	126	84	-
Basin A	Z ₂	1.003	1.000	-	1.087	1.005	1.000	-	126	-	78	39	26	-
	Z ₃	1.003	-	-	1.085	-	-	-	-	-	1	-	-	-
	ΣR_i								931	-	721	592	394	-
Bédard	Z ₁	1.003	1.000	-	1.074	-	-	-	165	-	100	-	-	-
	Z ₂	1.003	-	0.984 ^a	1.074	-	-	-	72 ^b	145 ^b	50	-	-	-
	Z ₃	1.003	-	-	1.074	-	-	0.995	-	-	5	-	-	8
	ΣR_i								853	522	612	-	-	114

790 ^athe optimal value of α_2 , given here is for a COS value of -1.5, varies slightly with the COS value (see section S2.2.2.3 of the SI).

^bthe value of R₁ and R₂, given here is for a COS value of -1.5, varies with the COS value (see section S2.2.2.3 of the SI).



795

Table 4: Net reaction rates ($R_{\text{net}}^{\text{solute}}$; $\text{fmol cm}^{-3} \text{ s}^{-1}$) of CH_4 , DIC and oxidants in the zone with the highest production rate of CH_4 as well as the O_2 concentration in the bottom water ($[\text{O}_2]$ in mg L^{-1}), the R_2 rates ($\text{fmol cm}^{-3} \text{ s}^{-1}$) and the average carbon oxidation state (COS) of the fermenting OM at the origin of CH_4 calculated with Eq. (12) at both study sites, Lake Tantaré Basin B (Fig. 1), Jacks Lake (Carignan and Lean 1991) and Lake Lugano (Lazzaretti-Ulmer & Hanselmann 1999) for various sampling dates.

Lake Basin	Sampling date	$[\text{O}_2]$	$R_{\text{net}}^{\text{DIC}}$	$R_{\text{net}}^{\text{CH}_4}$	$R_{\text{net}}^{\text{Ox}}$	R_2	Reference	COS^a	
								Min.	Max.
Tantaré Basin A, 15 m	Oct 2015 – Z_1	3.5	223	-7	-335	0	this study	-3.2	-3.2
	Oct 2015 – Z_2	3.5	113	39	-103	0	this study	-0.9	-0.9
	Jul 2012	6.0	143	245	-66	-	1	-2.1	-1.7
	Sep 2006	4.0	89	33	-45	-	1	0.4	0.6
	Oct 2005	3.1	202	48	-44	-	1	1.8	2.1
	Sep 2004	4.6	99	45	-60	-	1	-0.3	-0.2
Tantaré Basin B, 22 m	Oct 2014	< 0.1	42	116	-1	-	2	-1.9	-1.9
	Oct 2011	0.4	279	783	-12	-	1	-2.0	-1.9
	Jul 2007	4.1	283	1147	-20	-	1	-2.5	-2.5
	Oct 2006	< 0.1	442	825	-2	-	1	-1.2	-1.2
Bédard, 10 m	Oct 2015 – Z_1	< 0.1	65	100	-6.5	0	this study	-1.1	-1.0
	Oct 2003	< 0.1	205	408	-13	-	3	-1.4	-1.4
Jacks Lake, 15 m	Sep 1981	na	284	514	-	-	4	-1.2	-1.2
Jacks Lake, 22 m	Sep 1981	na	904	2030	-	-	4	-1.5	-1.5
Lugano, Melide, 85 m	Mar 1989	2.0	228	388	-83	-	5	-1.8	-1.6
Lugano, Melide, 85 m	Jun 1989	< 0.1	45	97	-1	-	5	-1.5	-1.5
Lugano, Figino, 95 m	Mar 1989	4.0	1168	1903	-234	-	5	-1.4	-1.3
Lugano, Figino, 95 m	Jun 1989	< 0.1	237	355	-19	-	5	-1.0	-0.9

^a Minimum and Maximum COS values were obtained by setting χ_M to 0 and 1 in Eq. (12), except for Tantaré Basin A in October 2015 for which χ_M is known to be 0.75.

800 References: (1) Clayer et al. (2016), (2) Clayer et al. (2018), (3) see Supporting Information, (4) Carignan and Lean (1991), (5) Lazzaretti-Ulmer & Hanselmann (1999).